Supplementary Data

Multimodal NIR-Emitting PluS Silica Nanoparticles with Fluorescent, Photoacoustic and Photothermal Capabilities

Stefania Biffi*, Luca Petrizza, Chiara Garrovo, Enrico Rampazzo, Laura Andolfi, Pierangela Giustetto, Ivaylo Nicolov, Gabor Kurdi, Miltcho Danailov, Giorgio Zauli, Paola Secchiero, Luca Prodi*

Contents

Fluorophores Synthesis

Cy5 dye (**6**) was synthesized adapting reported procedures.[1]

^{13}C-NMR spectra of Cy dyes were obtained setting **D1 = 5 s**.

3-propyl-1,1,2-trimethyl-1H-benz[e]indolium iodide salt (2).

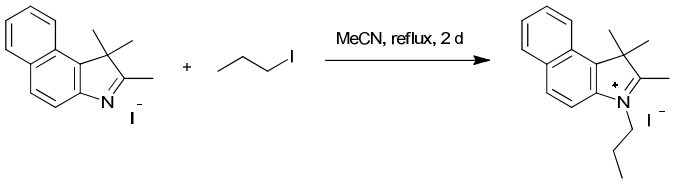

1 **2**

^{1}H-NMR (400 MHz, $CDCl_3$, 25°C) δ = 8.09 (2H, t, *J* = 8 Hz, ar. C*H*), 8.04 (1H, d, *J* = 8 Hz, ar. C*H*), 7.82 (1H, d, *J* = 8 Hz, ar. C*H*), 7.73 (1H, d, *J* = 8 Hz, ar. C*H*), 7.66 (1H, t, *J* = 8 Hz, ar. C*H*), 4.78 (2H, t, *J* = 8 Hz, -NC*H*$_2$-), 3.19 (3H, s, -NCC*H*$_3$), 2.10-2.05 (2H, m, -NCH$_2$C*H*$_2$CH$_3$), 1.87 (6H, s, -C*H*$_3$), 1.10 (3H, t, *J* = 8 Hz, -NCH$_2$CH$_2$C*H*$_3$).

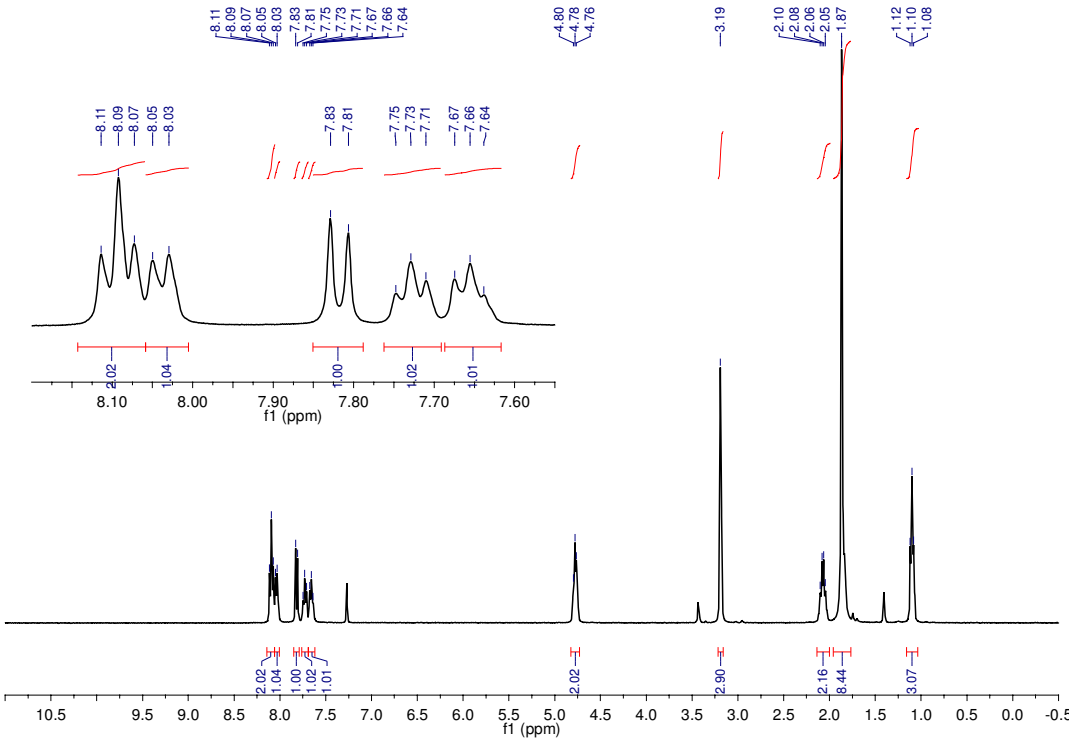

^{13}C-NMR (100 MHz, $CDCl_3$, 25°C) δ = 194.5, 137.2, 136.1, 132.6, 130.5, 129.0, 127.8, 126.7, 122.0, 112.0, 55.0, 50.3, 21.8, 20.9, 15.9, 10.5.

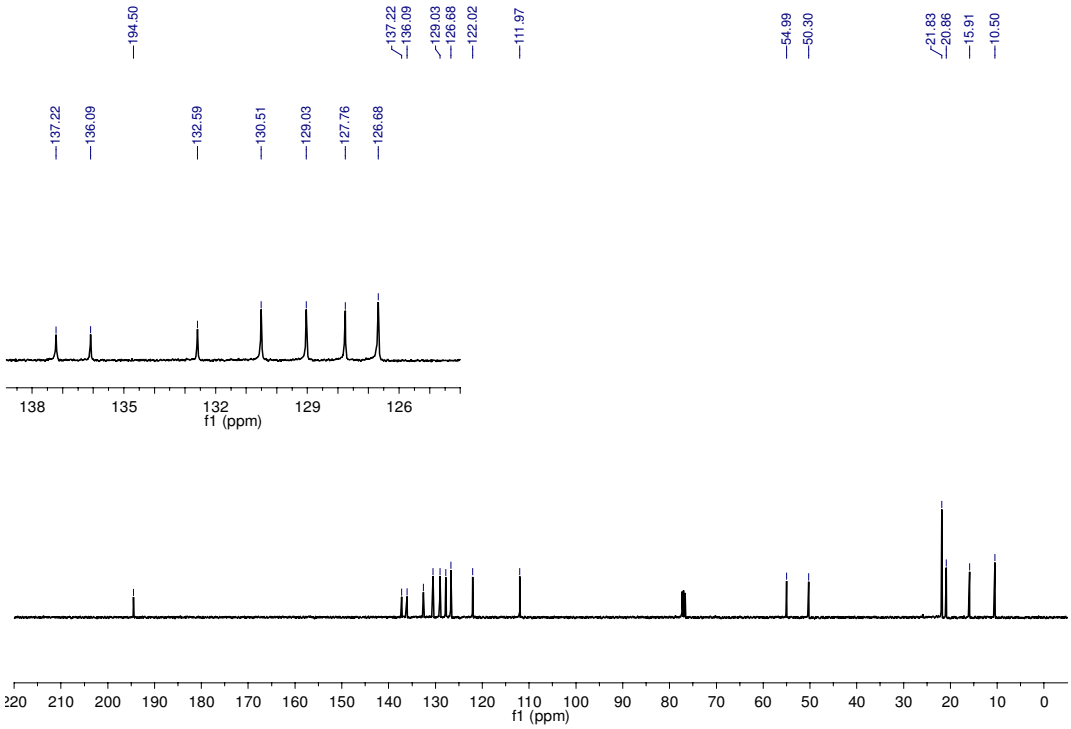

ESI-MS m/z calculated for $C_{18}H_{22}N^+$ 252.2; obs.: 252.2.

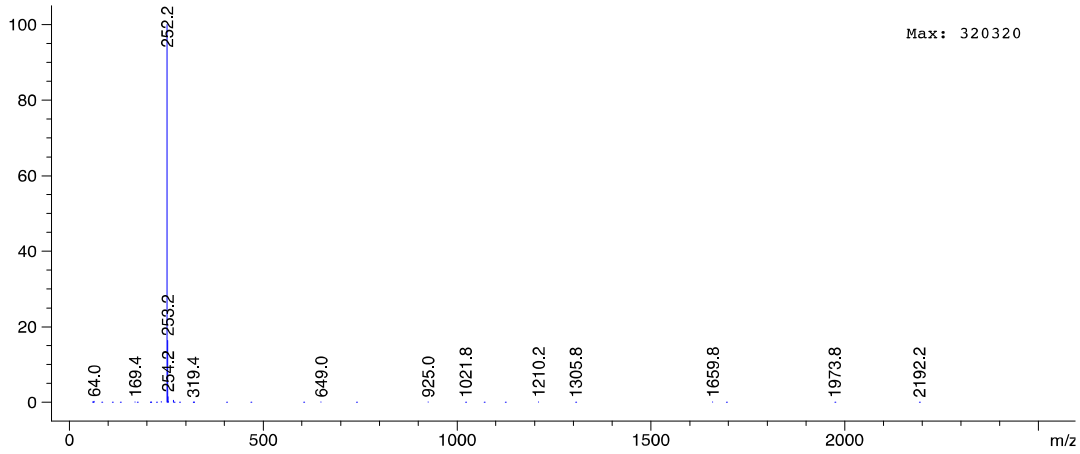

2-[4-(N-Phenyl-N-acetylamino)1,3-pentadienyl]-1,1-dimethyl-3-propyl-1H-benz[e]indolium iodide salt (3).

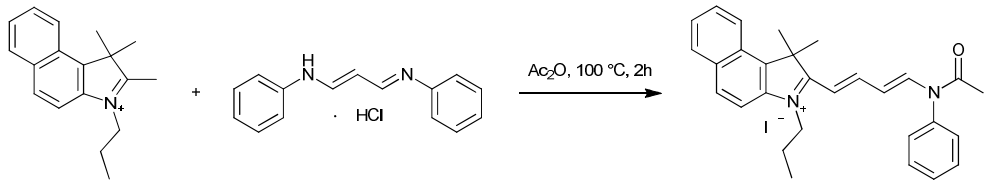

2 **3**

ESI-MS m/z calculated for $C_{29}H_{31}N_2O^+$ 423.24; obs.: 423.2.

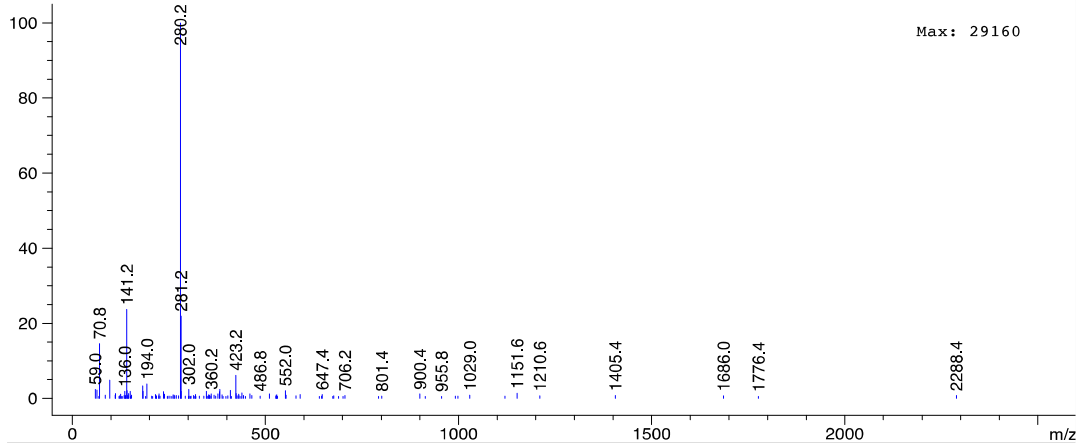

1,1,2-Trimethyl-3-(6-carboxylatohexyl)benz[e]indolium bromide salt (4).

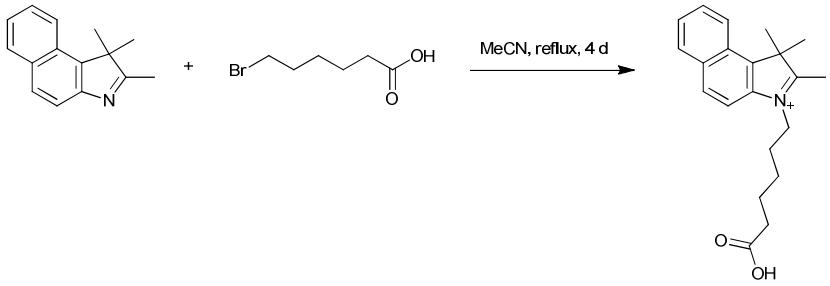

1 **4**

^{1}H-NMR (400 MHz, CD_3OD, 25°C) δ = 8.33 (1H, d, *J* = 8 Hz, ar. C*H*), 8.25 (1H, d, *J* = 8 Hz, ar. C*H*), 8.17 (1H, d, *J* = 8 Hz, ar. C*H*), 8.01 (1H, d, *J* = 8 Hz, ar. C*H*), 7.81 (1H, t, *J* = 8 Hz, ar. C*H*), 7.73 (1H, t, *J* = 8 Hz, ar. C*H*), 4.63 (2H, t, *J* = 8 Hz, -NC*H*$_2$-), 3.31 (3H, s, -NCC*H*$_3$) overlapped with the solvent residual signal, 2.36 (2H, t, *J* = 6 Hz, -C*H*$_2$COOH), 2.09-2.02 (2H, m, -NCH$_2$C*H*$_2$-), 1.85 (6H, s, -C*H*$_3$), 1.76-1.69 (2H, m, -C*H*$_2$CH$_2$COOH), 1.62-1-54 (2H, m, -CH$_2$C*H*$_2$CH$_2$-), 1.18 (3H, t, *J* = 8 Hz, -CH$_2$C*H*$_3$).

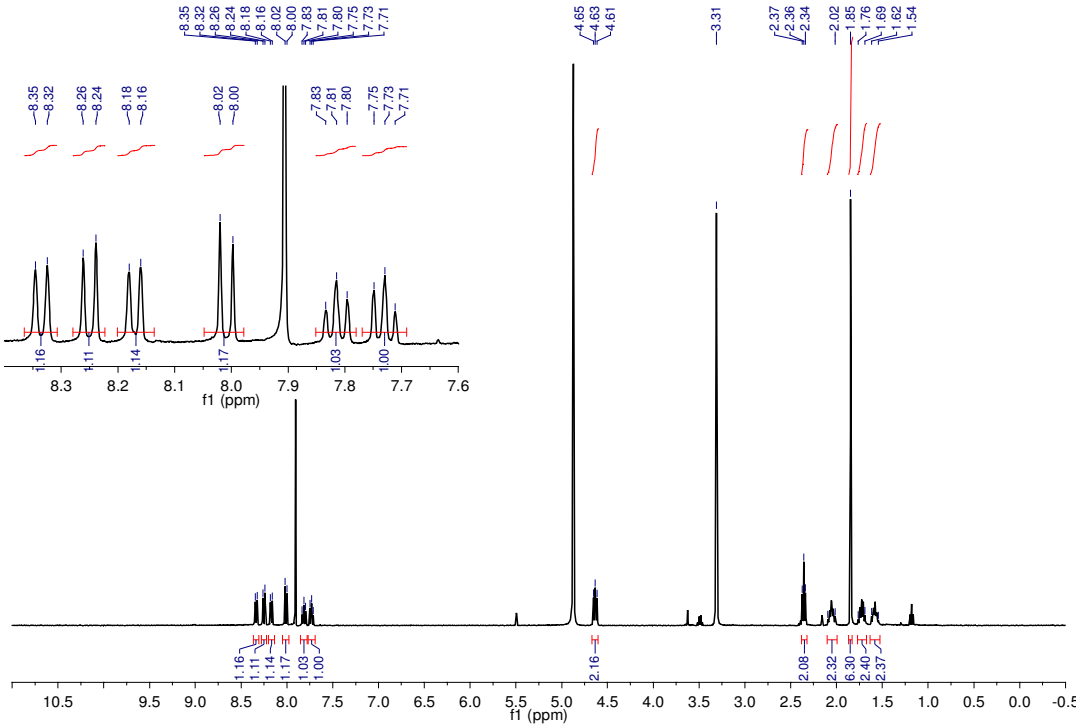

^{13}C-NMR (100 MHz, CD_3OD, 25°C) δ = 197.5, 177.1, 139.7, 138.7, 135.1, 132.4, 131.0, 129.7, 129.1, 128.7, 124.4, 113.8, 57.3, 34.4, 28.7, 27.0, 25.4, 22.4, 13.8.

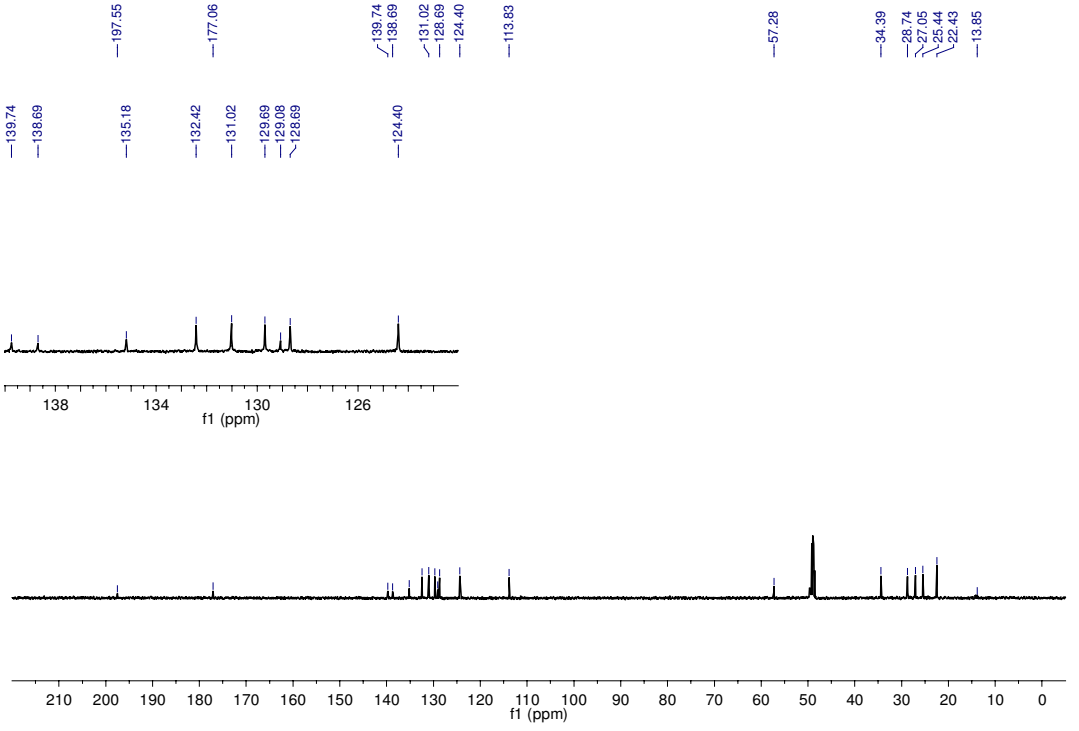

ESI-MS m/z calculated for $C_{21}H_{26}NO_2^+$ 324.2; obs.: 324.2.

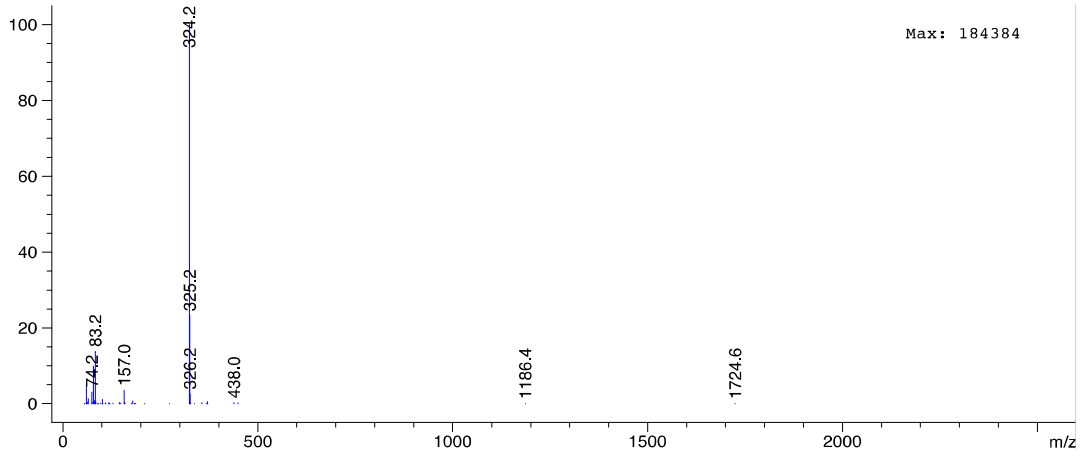

2-[7-(1,3-Dihydro-1,1-dimethyl-3-propylbenz[e]indolin-2-ylidene)-1,3,5-pentatrienyl]-1,1-dimethyl-3-(6-carboxylatohexyl)-1H-benz[e]indolium inner salt (5).

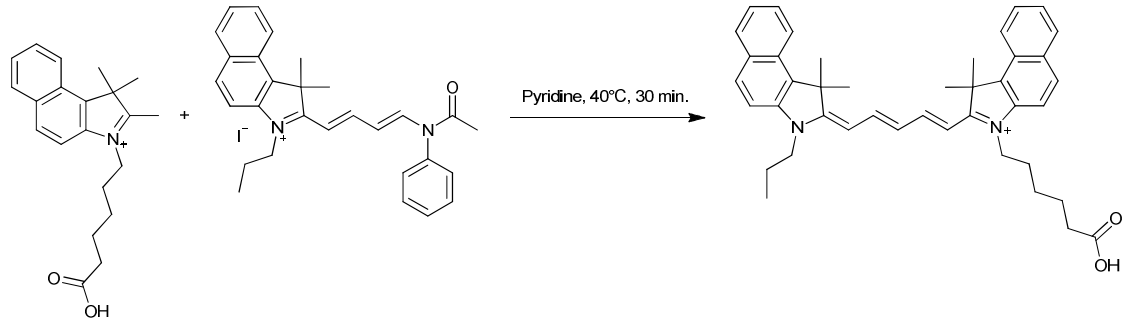

4 **3** **5**

^{1}H-NMR (400 MHz, CD_3OD, 25°C) δ = 8.35 (2H, t, *J* = 14 Hz, ar. C*H*), 8.25 (2H, d, *J* = 8 Hz, ar. C*H*), 8.00 (4H, t, *J* = 10 Hz, ar. C*H*), 7.65 (2H, t, *J* = 8 Hz, ar. C*H*), 7.59 (2H, d, *J* = 4 Hz, ar. C*H*), 7.49 (2H, t, *J* = 8 Hz, C*H*), 6.68 (1H, t, *J* = 14 Hz, C*H*), 6.37-6.32 (2H, m, C*H*), 4.25-4.19 (4H, m, -NC*H*$_2$-), 2.31 (2H, t, *J* = 8 Hz, -C*H*$_2$COOH), 2.03 (12H, s, -C*H*$_3$), 1.95-1.87 (4H, m, -NCH$_2$C*H*$_2$-), 1.76-1.68 (2H, m, -C*H*$_2$CH$_2$COOH), 1.59-1-51 (2H, m, -CH$_2$C*H*$_2$CH$_2$-), 1.10 (2H, t, *J* = 8 Hz, -CH$_2$C*H*$_3$).

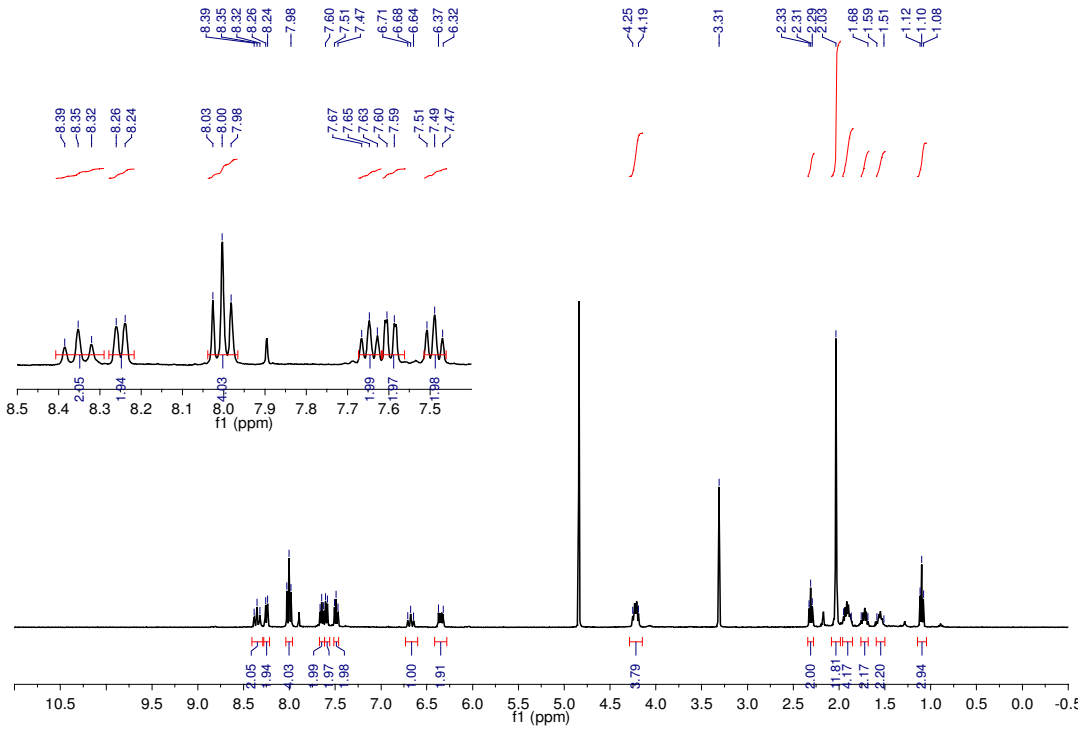

^{13}C-NMR (100 MHz, CD_3OD, 25°C) δ = 178.3, 176.1, 175.9, 154.3, 141.1, 135.1, 133.4, 131.7, 131.0, 129.5, 128.7, 126.5, 126.1, 123.3, 112.1, 104.0, 52.4, 46.4, 45.0, 35.5, 28.5, 27.6, 27.7, 26.0, 22.1, 11.5.

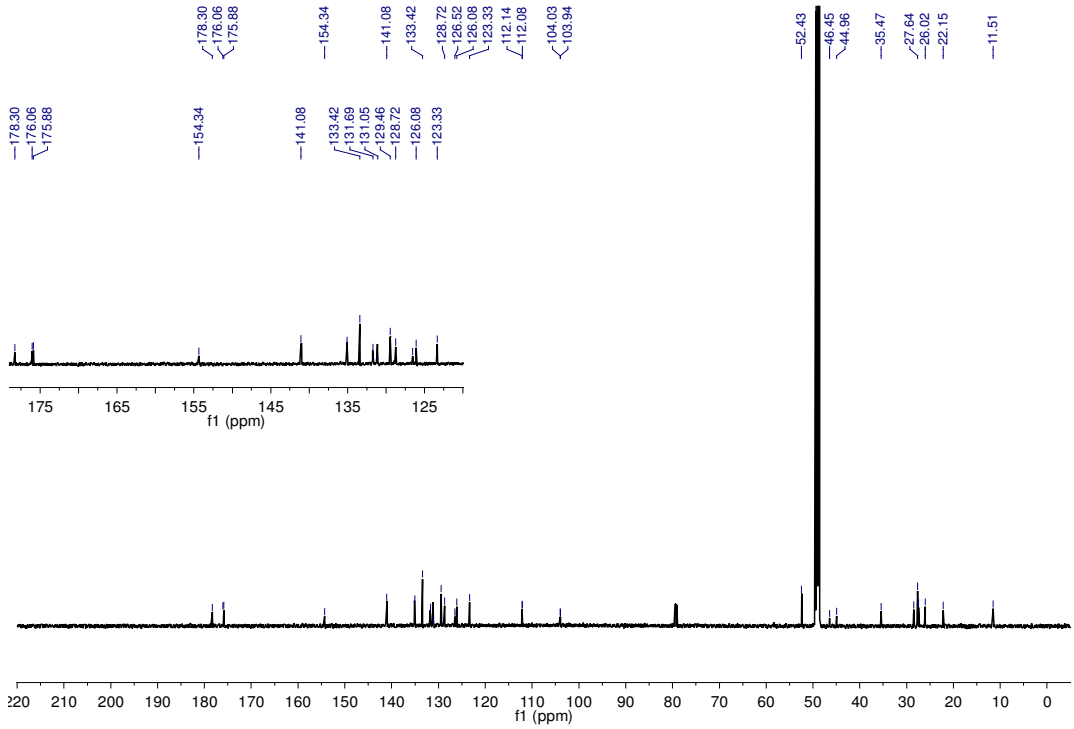

ESI-MS m/z calculated for $C_{42}H_{47}N_2O_2^+$ 611.4; obs.: 611.2.

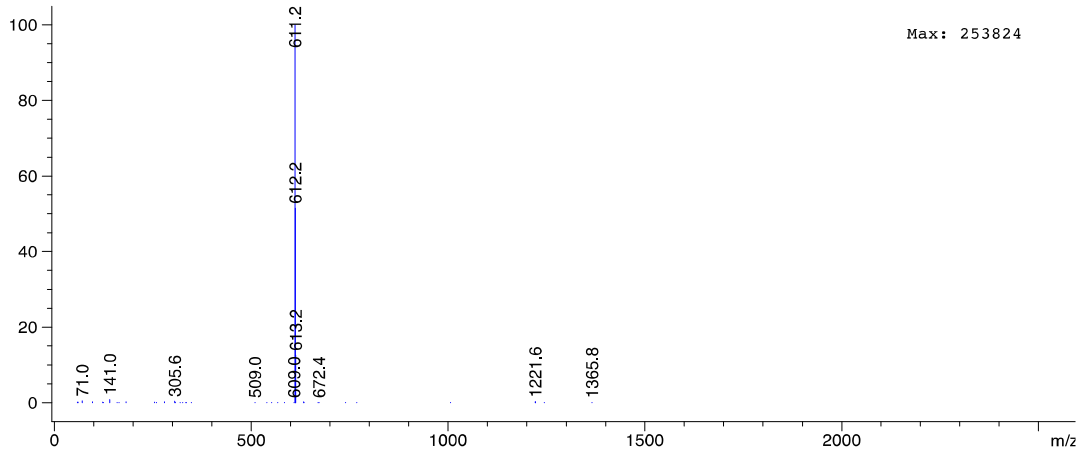

2-[7-(1,3-Dihydro-1,1-dimethyl-3-propylbenz[e]indolin-2-ylidene)-1,3,5-pentatrienyl]-1,1-dimethyl-3-[6-[*N*-(3-(triethoxysilyl)propyl]hexanamide]-1H-benz[e]indolium iodide salt (6).

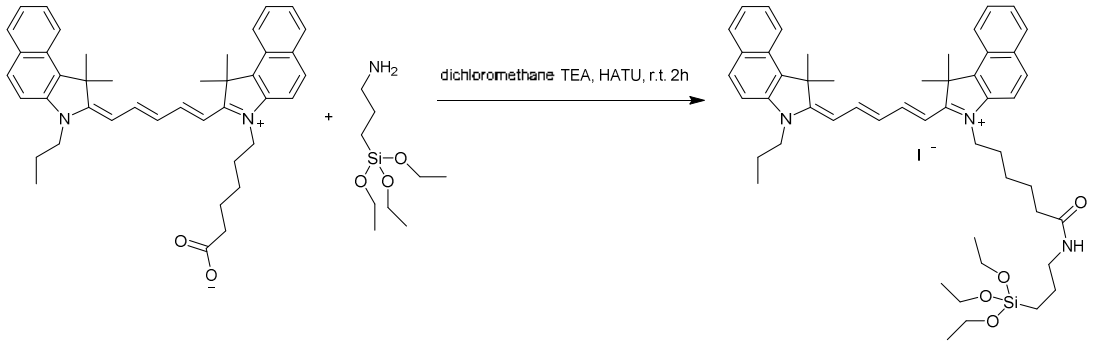

5 **6**

^{1}H-NMR (400 MHz, CD_3OD, 25°C) δ = 8.32-8.27 (2H, m, ar. C*H*), 8.20 (2H, d, *J* = 4 Hz, ar. C*H*), 7.98 (2H, d, *J* = 8 Hz, ar. C*H*), 7.94 (2H, d, *J* = 4 Hz, ar. C*H*), 7.61 (2H, t, *J* = 6 Hz, ar. C*H*), 7.56 (2H, t, *J* = 6 Hz, ar. C*H*), 7.44 (2H, t, *J* = 6 Hz, C*H*), 6.67 (1H, t, *J* = 10 Hz, C*H*), 6.33-6.28 (2H, m, C*H*), 4.20-4.16 (4H, m, -NC*H*$_2$-), 3.78 (6H, q, *J* = 4 Hz, -OC*H*$_2$-), 3.10 (2H, t, *J* = 4 Hz, -NHC*H*$_2$-), 2.21 (2H, t, *J* = 4 Hz, -C*H*$_2$CONH-), 1.97 (12H, s, -C*H*$_3$), 1.91-1.84 (4H, m, -NCH$_2$C*H*$_2$-), 1.73-1.68 (2H, m, -C*H*$_2$CH$_2$CONH-), 1.57-1-53 (2H, m, -CH$_2$C*H*$_2$CH$_2$-), 1.51-1.47 (2H, m, -NHCH$_2$C*H*$_2$-), 1.17 (9H, t, *J* = 6 Hz, -OCH$_2$C*H*$_3$), 1.08 (3H, t, *J* = 4 Hz, -CH$_2$CH$_2$C*H*$_3$), 0.58-0.55 (2H, m, -SiC*H*$_2$).

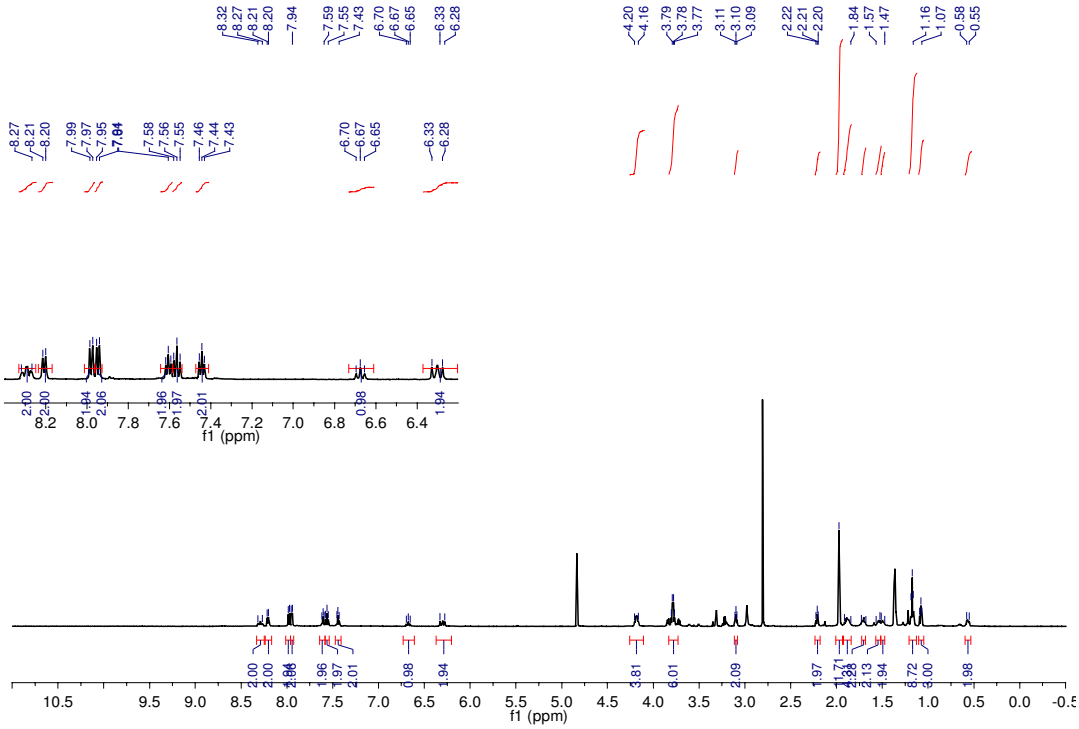

^{13}C-NMR (100 MHz, CD_3OD, 25°C) δ = 176.1, 175.7, 167.4, 163.1, 154.3, 135.2, 133.3, 131.6, 131.0, 129.4, 128.7, 126.7, 126.0, 123.3, 112.1, 104.0, 59.5, 55.8, 52.3, 46.4, 44.9, 43.8, 43.0, 38.9, 36.7, 28.4, 27.6, 26.6, 22.1, 18.7, 17.2, 13.1.

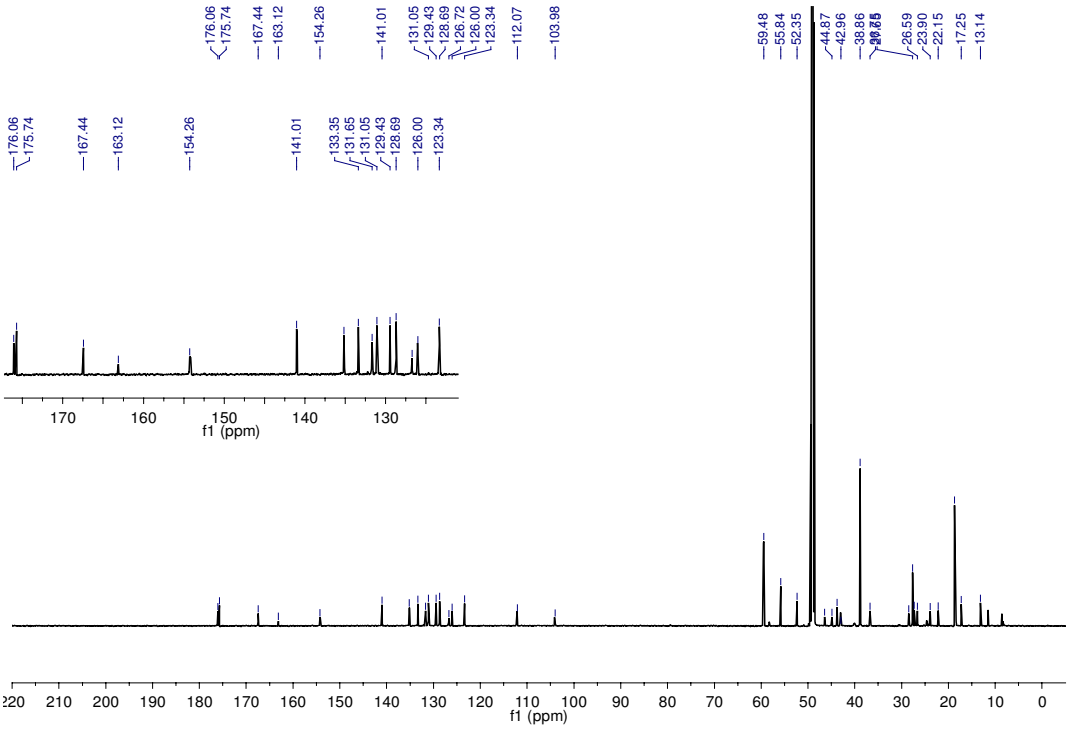

ESI-MS m/z calculated for $C_{51}H_{68}N_3O_4Si^+$ 814.5; obs.: 814.4.

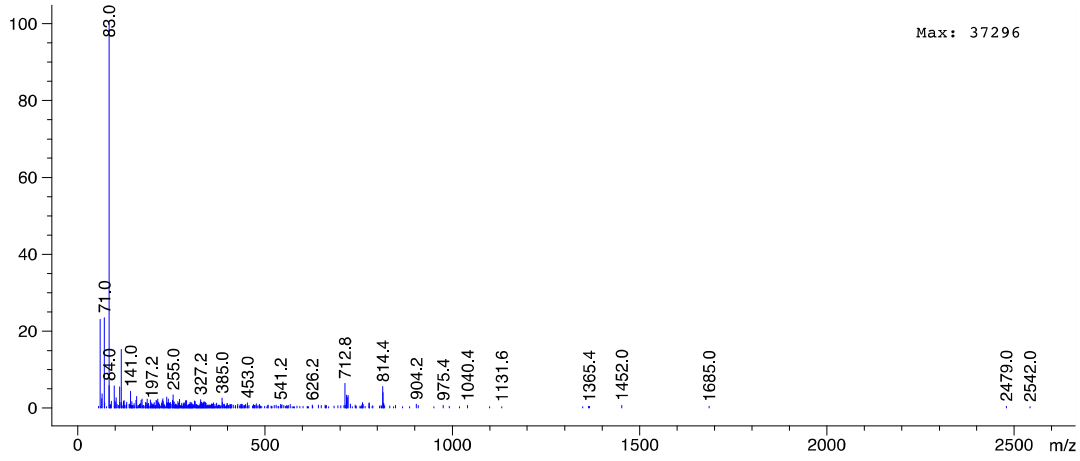

Synthesis of Cy7 (7)

2-[2-[2-Thio-[3-(triethoxysilyl)propyl]-3-[2-(1,3-dihydro-1,1,3-trimethyl-2*H*-benzo[e]-indol-2-ylidene)-ethylidene]-1-cyclohexen-1-yl]-ethenyl]-1,1,3-trimethyl-1*H*-benzo[e]indolium perchlorate (7).

Compound **7** was synthesized starting from Cy7 dye IR813, 3-mercaptopropionic acid and 3-aminopropyltriethoxysilane adapting reported procedures.[2]

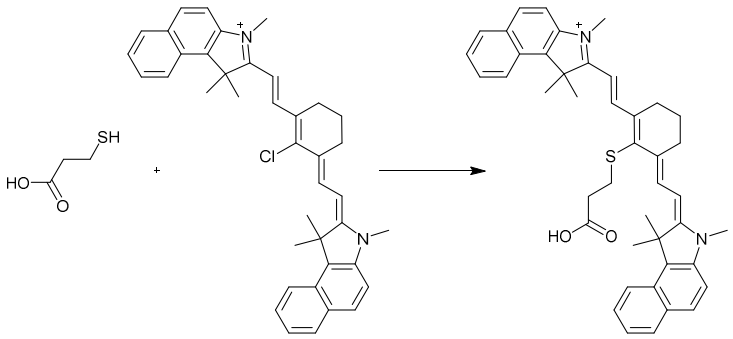

IR 813

^{1}H-NMR (600 MHz, CD_3OD, 25°C) δ = 9.06 (2H, d, *J* = 12 Hz, C*H*), 8.29 (2H, d, *J* = 12 Hz, ar. C*H*), 8.02 (2H, d, *J* = 6 Hz, ar. C*H*), 7.99 (2H, d, *J* = 6 Hz, ar. C*H*), 7.64 (2H, t, *J* = 9 Hz, ar. C*H*), 7.60 (2H, d, *J* = 12 Hz, ar. C*H*), 7.48 (2H, t, *J* = 6 Hz, ar. C*H*), 6.30 (2H, d, *J* = 12 Hz, C*H*), 3.77 (6H, s, -NCH_3), 3.12 (2H, t, *J* = 9 Hz, -SCH_2-), 2.73 (4H, t, *J* = 6 Hz, -CCH_2CH_2-), 2.53 (2H, t, *J* = 9 Hz, -CH_2COOH), 2.07 (12H, s, -CCH_3), 1.99-1.95 (2H, m, -CCH$_2$CH_2-).

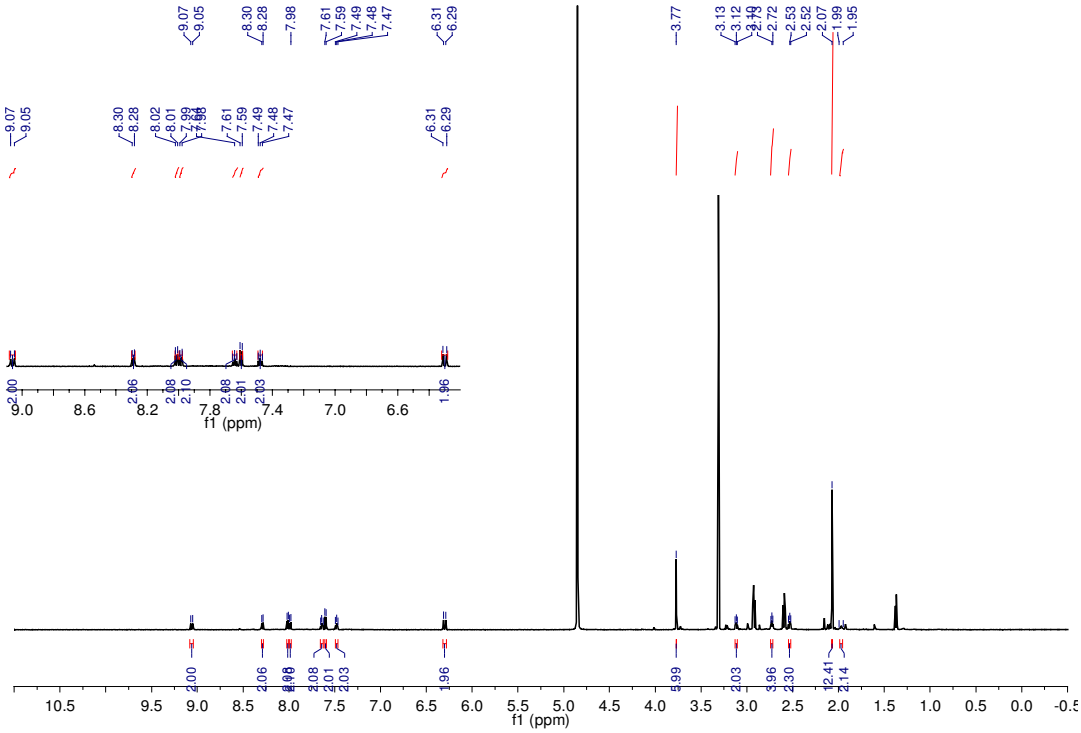

^{13}C-NMR (100 MHz, CD_3OD, 25°C) δ = 178.6, 175.9, 144.8, 142.2, 141.8, 138.4, 134.8, 134.6, 134.5, 133.4, 131.1, 129.5, 128.7, 125.9, 123.5, 111.8, 106.4, 52.2, 39.7, 37.7, 35.8, 27.8.

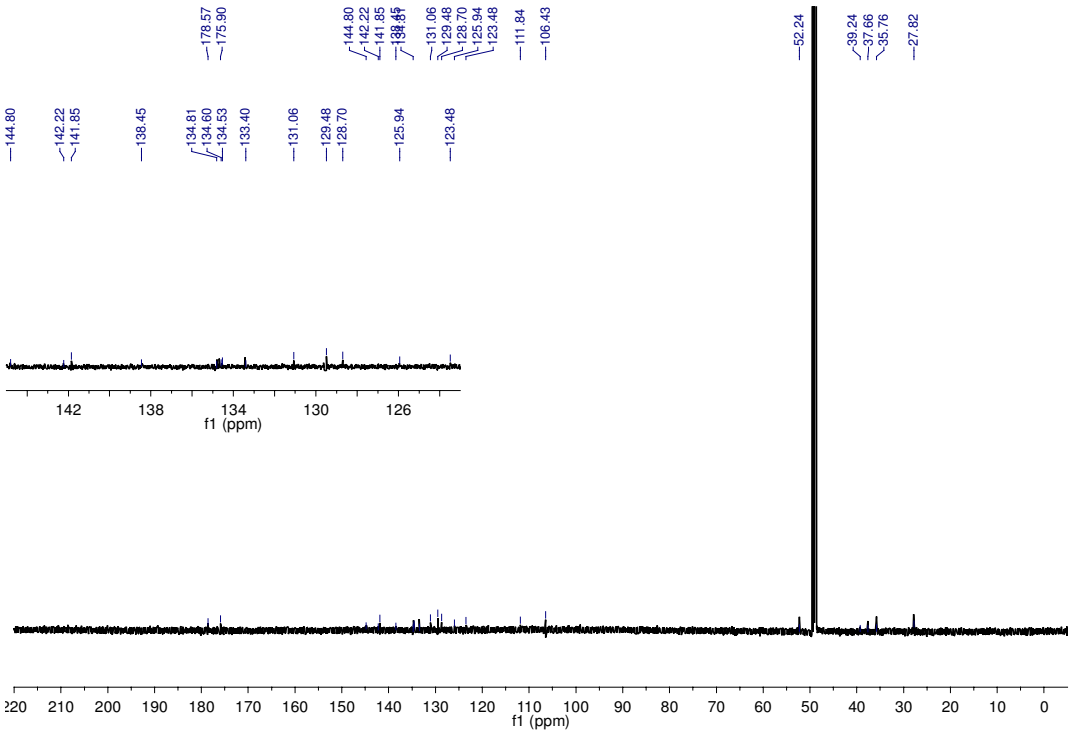

ESI-MS m/z calculated for $C_{43}H_{45}N_2O_2S^+$ 653.3; 653.4.

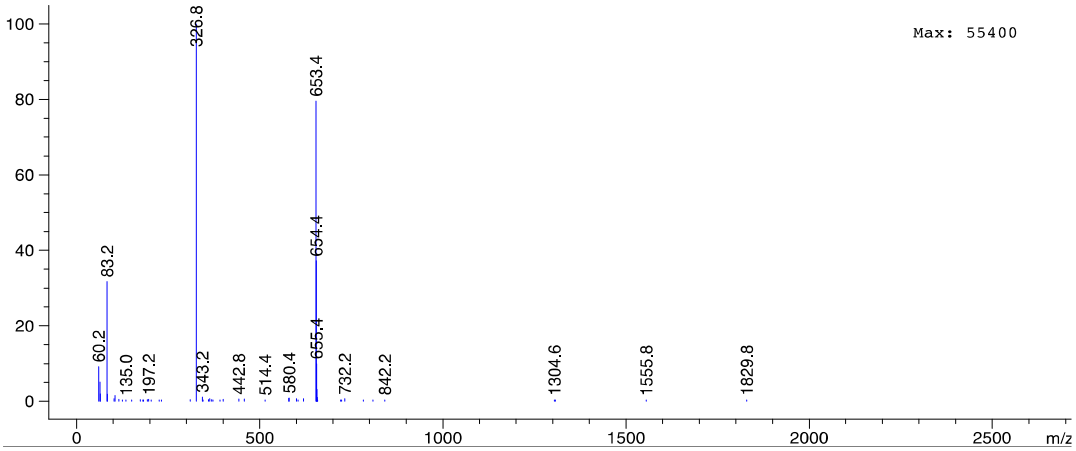

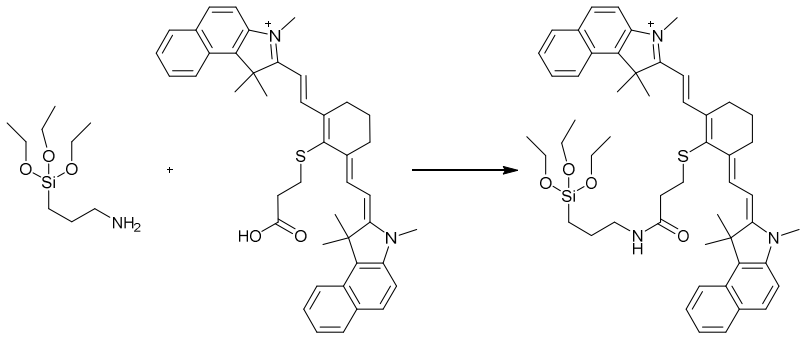

7

^{1}H-NMR (600 MHz, CD_3OD, 25°C) δ = 9.00 (2H, d, *J* = 12 Hz, C*H*), 8.27 (2H, d, *J* = 12 Hz, ar. C*H*), 8.02 (2H, d, *J* = 6 Hz, ar. C*H*), 8.00 (2H, d, *J* = 6 Hz, ar. C*H*), 7.65 (2H, t, *J* = 6 Hz, ar. C*H*), 7.61 (2H, d, *J* = 12 Hz, ar. C*H*), 7.48 (2H, t, *J* = 9 Hz, ar. C*H*), 6.31 (2H, d, *J* = 12 Hz, C*H*), 3.77 (6H, s, -NCH_3), 3.74-3.70 (6H, q, *J* = 6 Hz, -OCH_2-), 3.17-3.13 (2H, m, -SCH_2-) + (2H, m, -NHCH_2-) overlapped, 2.73 (4H, t, *J* = 6 Hz, -CCH_2CH$_2$-), 2.58 (2H, t, *J* = 9 Hz, -CH_2CONH-), 2.06 (12H, s, -CCH_3), 1.99-1.97 (2H, m, -CCH$_2$CH_2-), 1.59-1.53 (2H, m, -SiCH$_2$CH_2-), 1.10 (9H, t, *J* = 6 Hz, -OCH$_2$CH_3-), 0.59-0.56 (2H, m, -SiCH_2-).

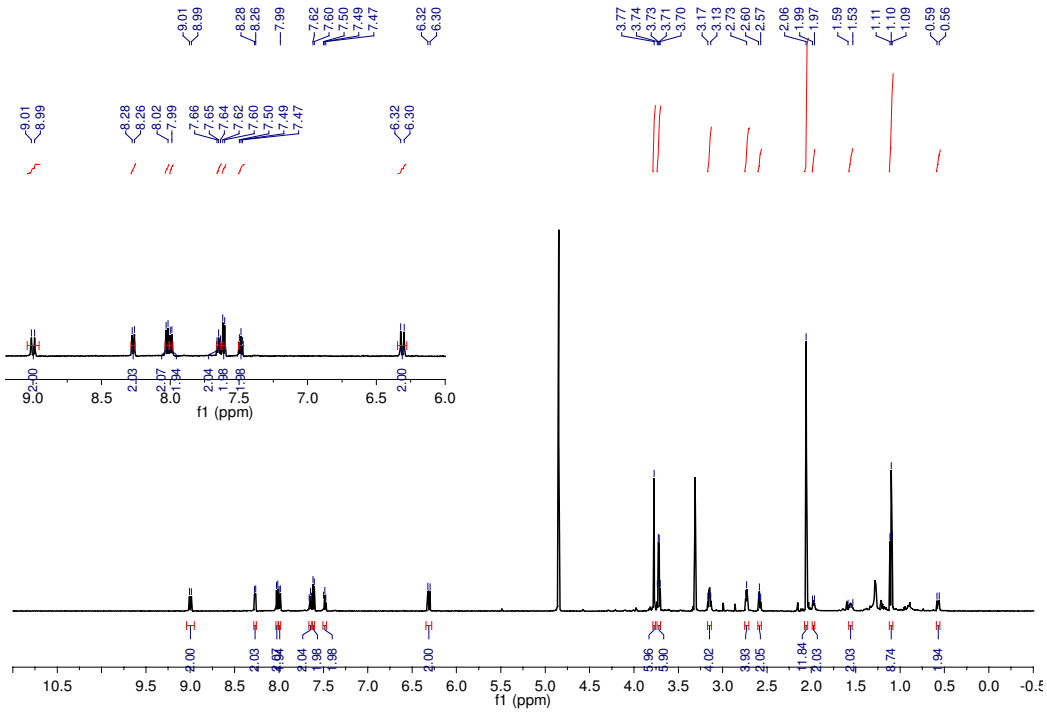

^{13}C-NMR (100 MHz, CD_3OD, 25°C) δ = 175.8, 172.9, 157.2, 146.2, 141.8, 134.7, 133.5, 131.7, 131.1, 129.4, 128.8, 126.0, 123.4, 111.9, 101.9, 59.5, 52.2, 43.2, 37.3, 34.5, 33.1, 31.9, 27.9, 27.3, 18.6, 14.3.

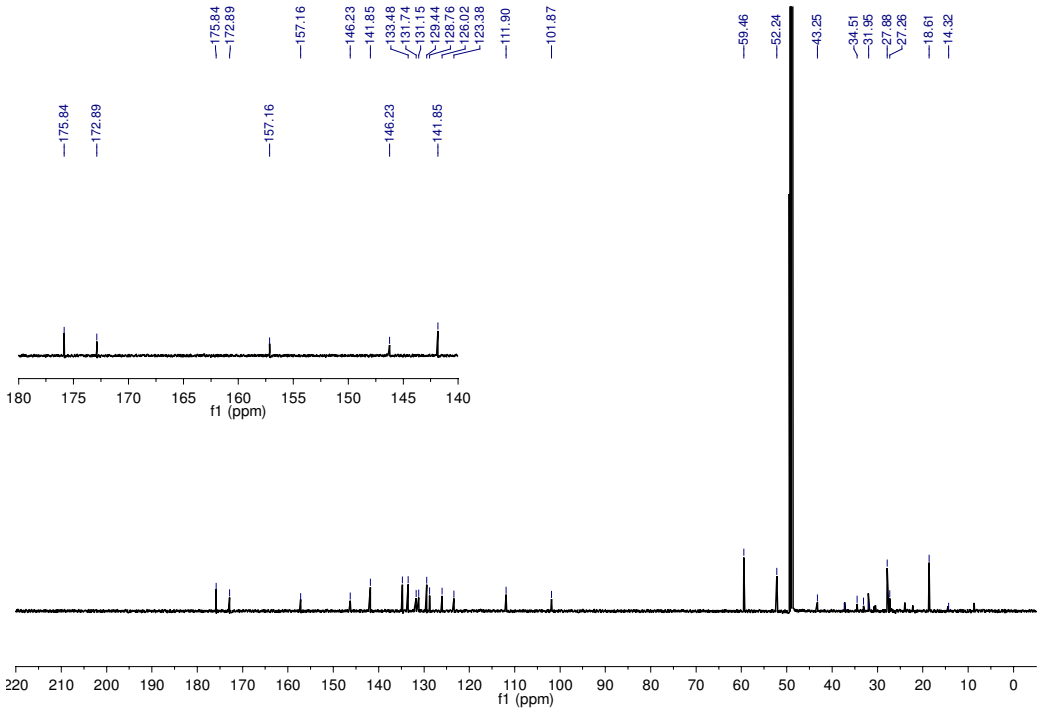

ESI-MS m/z calculated for $C_{52}H_{66}N_3O_4SSi^+$ 856.4; obs.: 856.6.

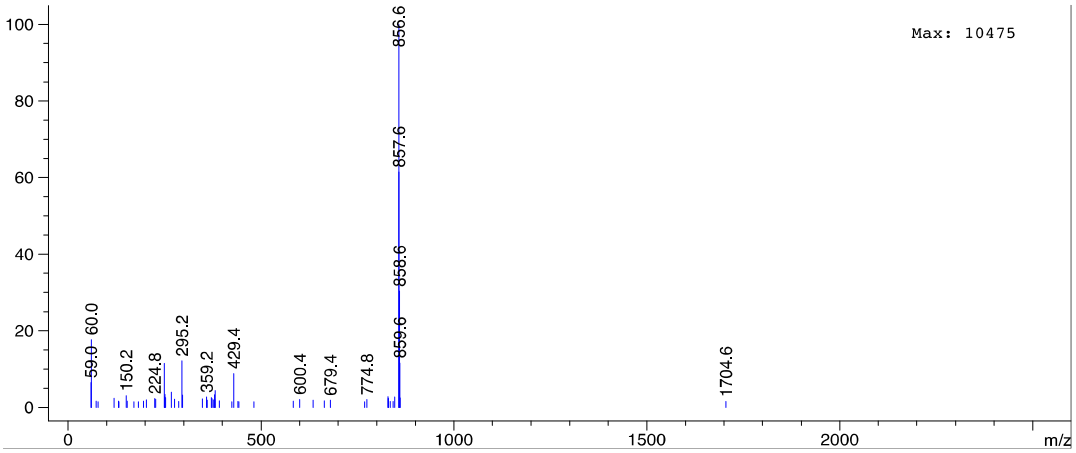

Photophysical measurements

UV-VIS absorption spectra were recorded at 25°C by means of Perkin-Elmer Lambda 45 spectrophotometer. The fluorescence spectra were recorded with a Perkin-Elmer Lambda LS 55 fluorimeter and with a modular UV-vis-NIR spectrofluorimeter Edinburgh Instruments FLS920

equipped with a photomultiplier Hamamatsu R928P. The latter instrument connected to a PCS900 PC card was used for the Time Correlated Single Photon Counting (TCSPC) experiments (excitation laser λ = 640 nm). Corrected fluorescence emission and excitation spectra (450 W Xe lamp) were obtained with the same instrument equipped with both a Hamamatsu R928P P photomultiplier tube (for the 500-850 nm spectral range) and an Edinburgh Instruments Ge detector (for the 800-1600 nm spectral range). Quartz cuvettes with optical path length of 1 cm were used for both absorbance and emission measurements.

Nanoparticles solutions were diluted with Milli-Q® water. Luminescence quantum yields (uncertainty ± 15%) were recorded on air-equilibrated solutions and cyanine IR-125 (from Acros Organics) in ethanol (Φ = 0.05).[3] Corrections for instrumental response, inner filter effects and phototube sensitivity were performed.[4]

Photophysical properties. The absorption and emission spectra of samples **NP-1**, **NP-2**, **NP-3**, **NP-4**, **NP-5**, **NP-6**, **NP-7** are reported in **Figure S2-8**.

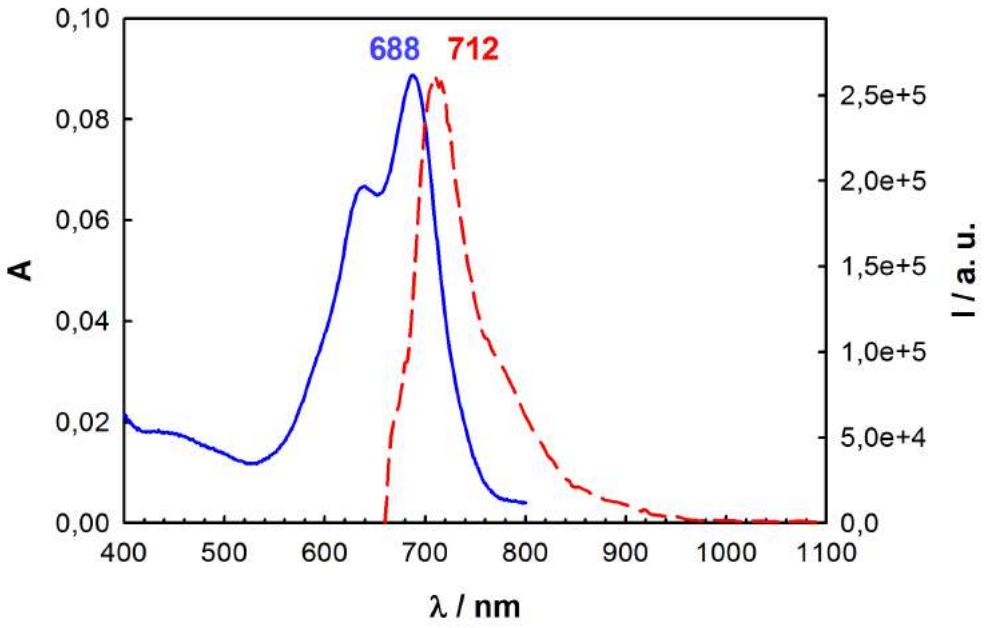

Figure S1: Absorption and corrected fluorescence emission spectra of sample **NP-1** (water, λ_{ex} = 650 nm, [**NP-1**] = 1.4 µM).

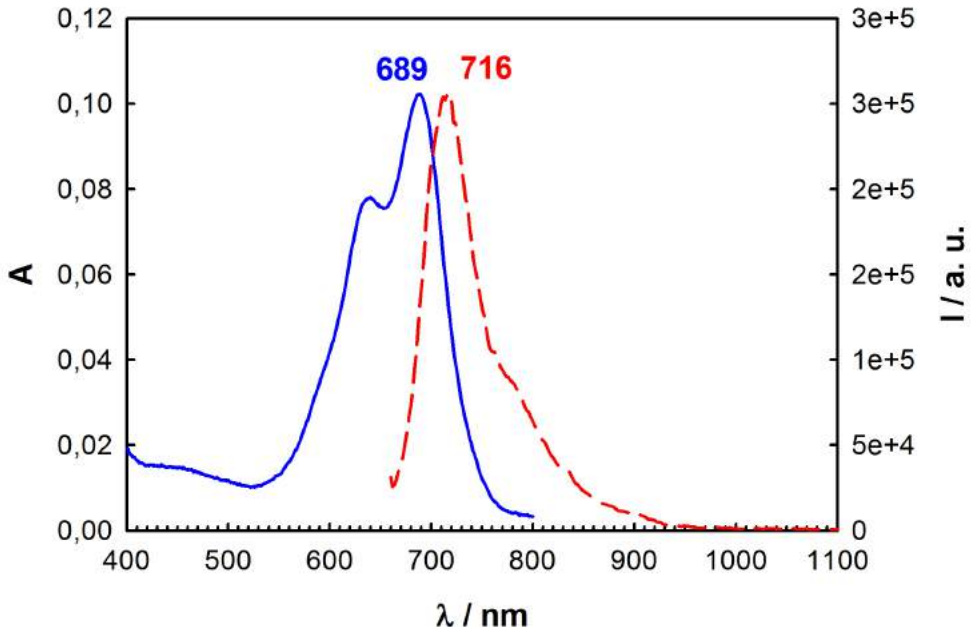

Figure S2: Absorption and corrected fluorescence emission spectra of sample **NP-2** (water, λ_{ex} = 650 nm, [**NP-2**] = 0.7 μM).

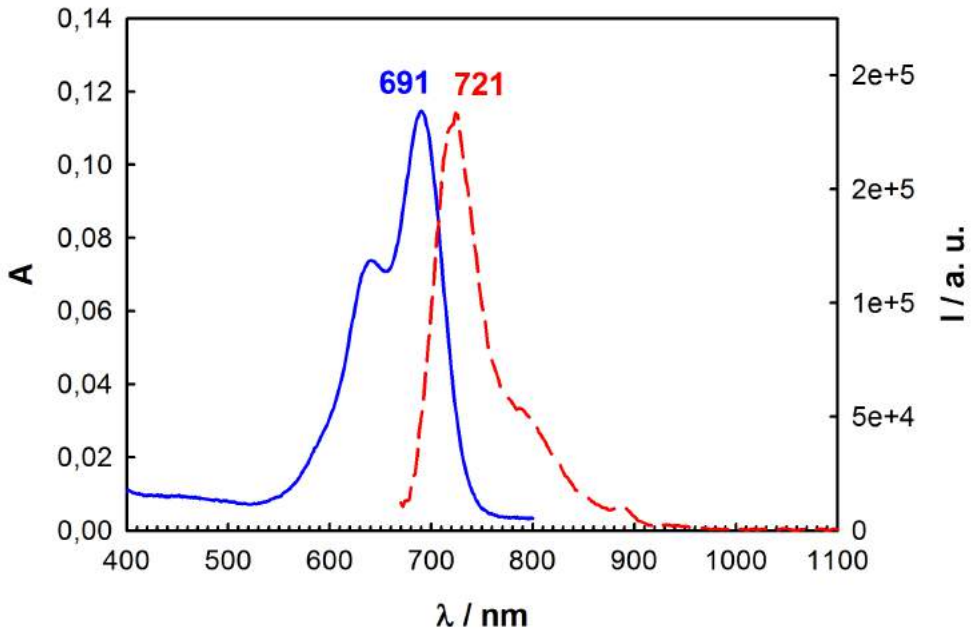

Figure S3: Absorption and corrected fluorescence emission spectra of sample **NP-3** (water, λ_{ex} = 650 nm, [**NP-3**] = 0.1 μM).

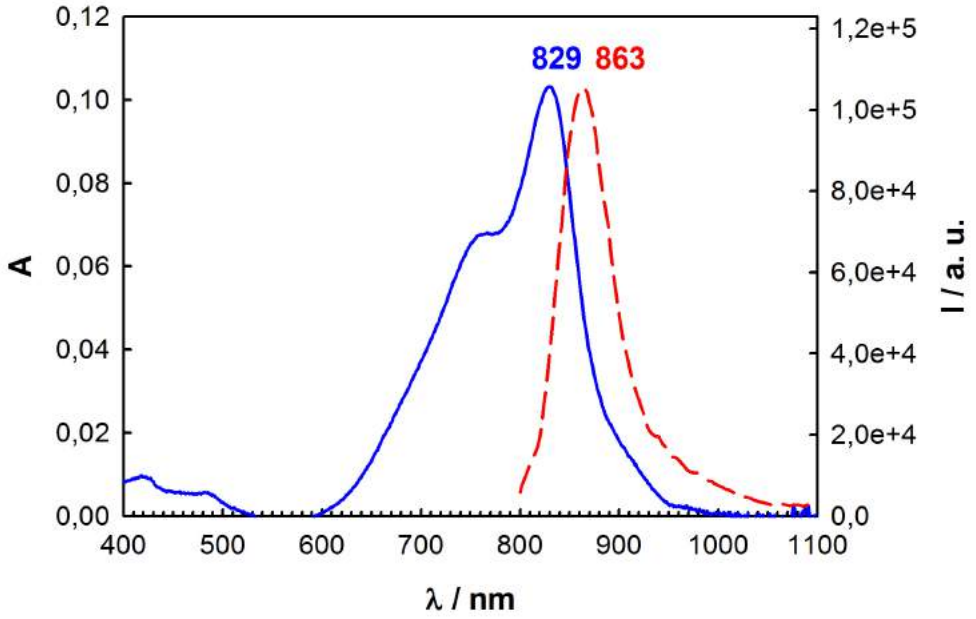

Figure S4: Absorption and corrected fluorescence emission spectra of sample **NP-4** (water, λ_{ex} = 750 nm, [**NP-4**] = 0.04 μM).

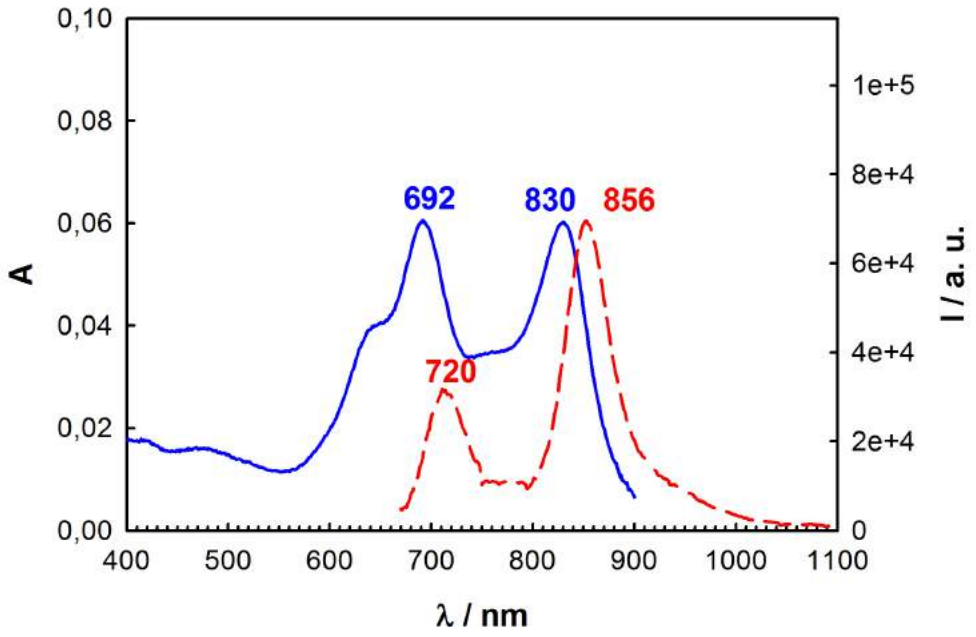

Figure S5: Absorption and corrected fluorescence emission spectra of sample **NP-5** (water, λ_{ex} = 640 nm, [**NP-5**] = 0.08 μM).

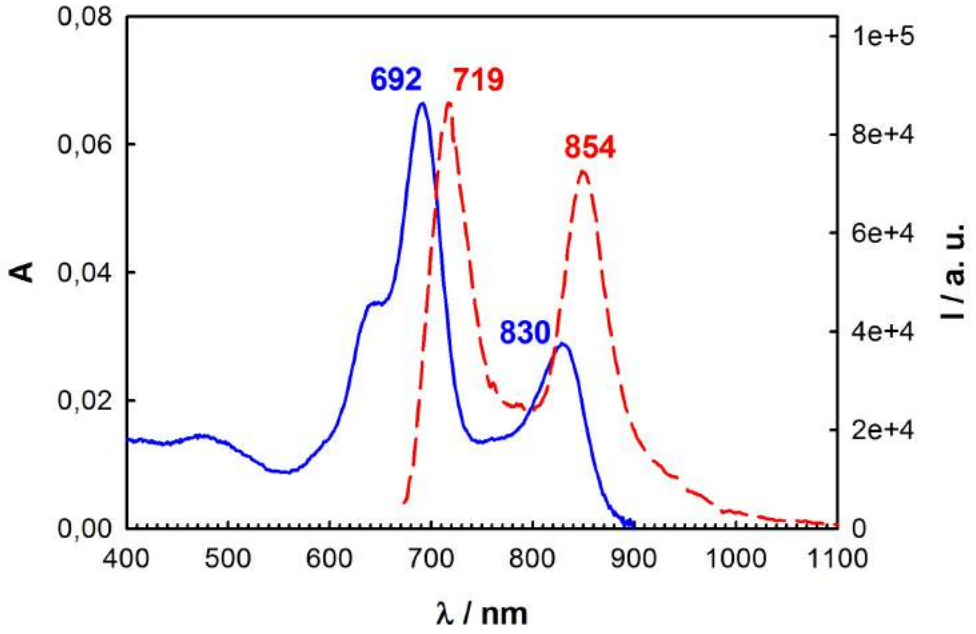

Figure S6: Absorption and corrected fluorescence emission spectra of sample **NP-6** (water, λ_{ex} = 640 nm, [**NP-6**] = 0.06 μM).

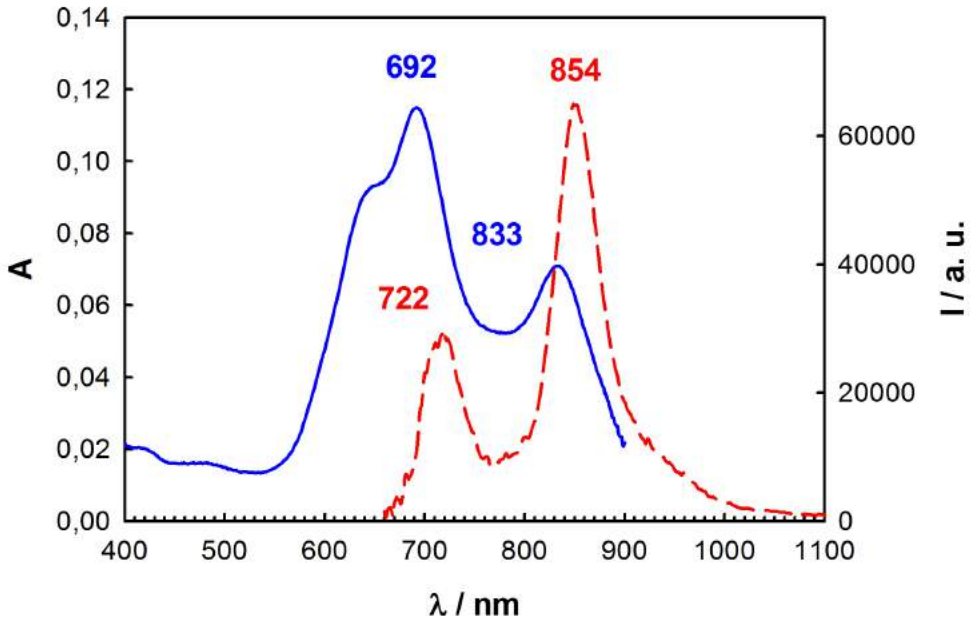

Figure S7: Absorption and corrected fluorescence emission spectra of sample **NP-7** (water, λ_{ex} = 640 nm, [**NP-7**] = 0.07 μM).

The efficiency of the energy transfer from Cy5.5 (**6**) to Cy7 (**7**) was evaluated using the following equation:

$$\eta_{ET} = 1 - \frac{\tau_{DA}}{\tau_D}$$

where τ_{DA} is the lifetime of the donor in the presence of the acceptor, and τ_D is the lifetime of the donor itself [5]. The energy transfer efficiencies for the samples **NP-5**, **NP-6** and **NP-7** are reported in **Table 2**.

Photoacoustic Phantom

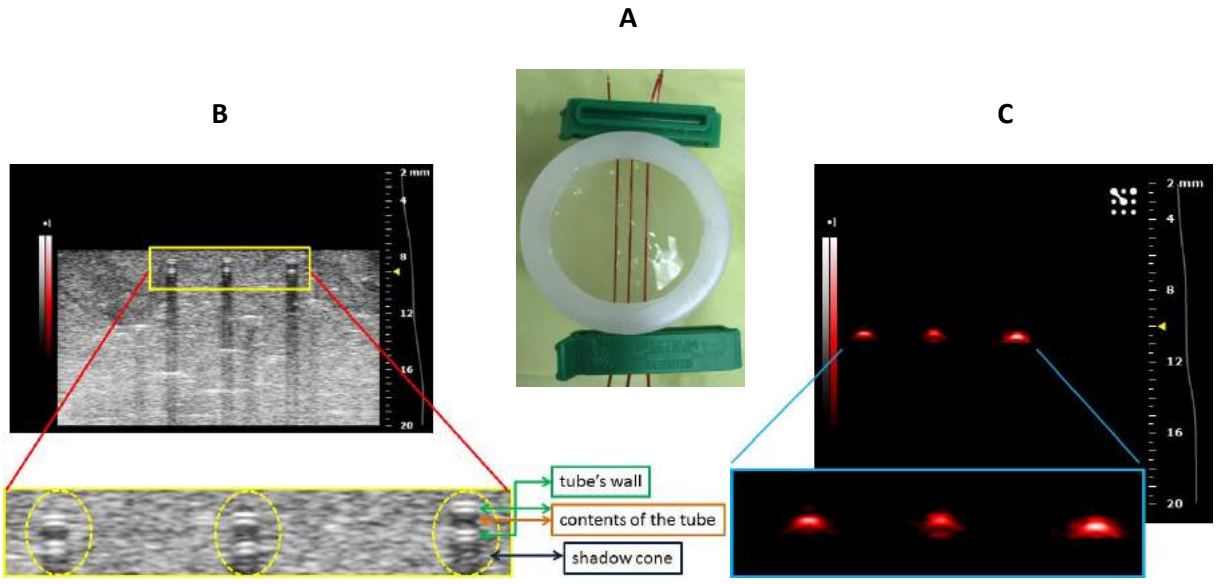

Figure S8. (**A**) Phantom structure used for PA *in vitro* experiments. (**B**) Phantom US image; axial tube section. The shadow cones projecting under the tubes are visible. (**C**) PA image signal of tested solution phantom image; axial view.

Trasmission Electron Microscopy (TEM) images

TEM images of NPs samples were obtained with a Philips CM 100 microscope, operating at 80 kV, and using 3.05 mm copper grids (Formvar support film - 400 mesh). A drop of NIR-PluS NPs solution diluted with water (1:50) was placed on the grid and then dried under vacuum. The TEM images showing the denser silica cores, were analyzed with the ImageJ software, considering several dozen to few hundred nanoparticles. The obtained histogram was fitted according to a Gaussian distribution obtaining the average diameter for the silica nanoparticles core.

Table S1: NIR-PluS NPs silica core mean diameter ± SD determined by TEM analysis.

Sample	*(d_{core} ± SD) [nm]*
NP-1	12 ± 2
NP-2	12 ± 1
NP-3	9.3 ± 1.5
NP-4	12.0 ± 1.5
NP-5	9.8 ± 1.5
NP-6	10.0 ± 1.5
NP-7	11 ± 2

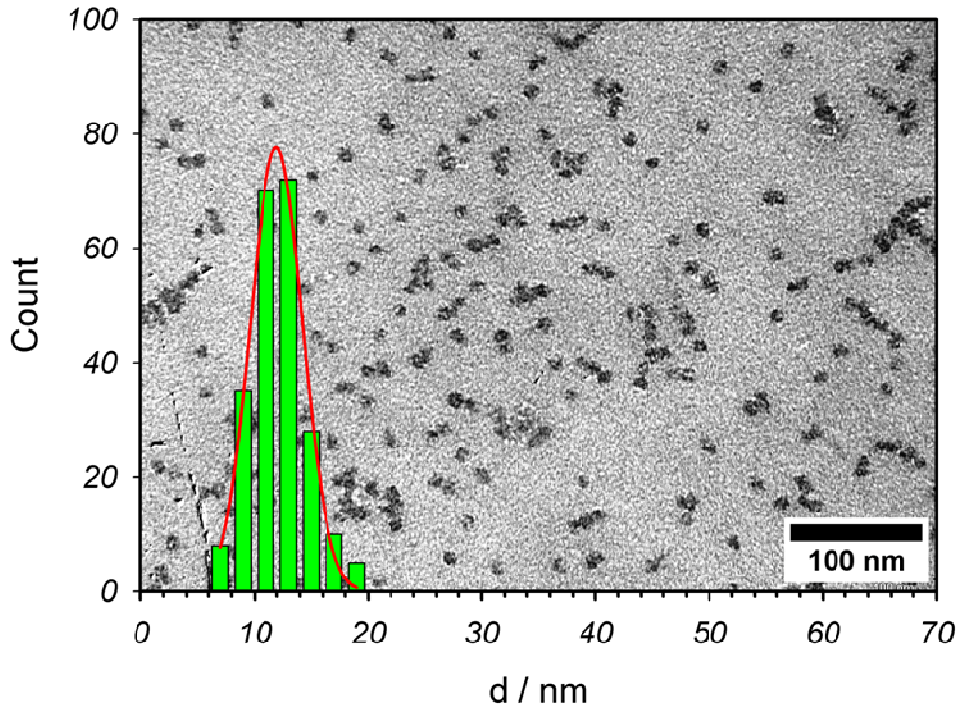

Figure S9: **NP-1**, TEM image and silica core size distribution: d = (12 ± 2) nm.

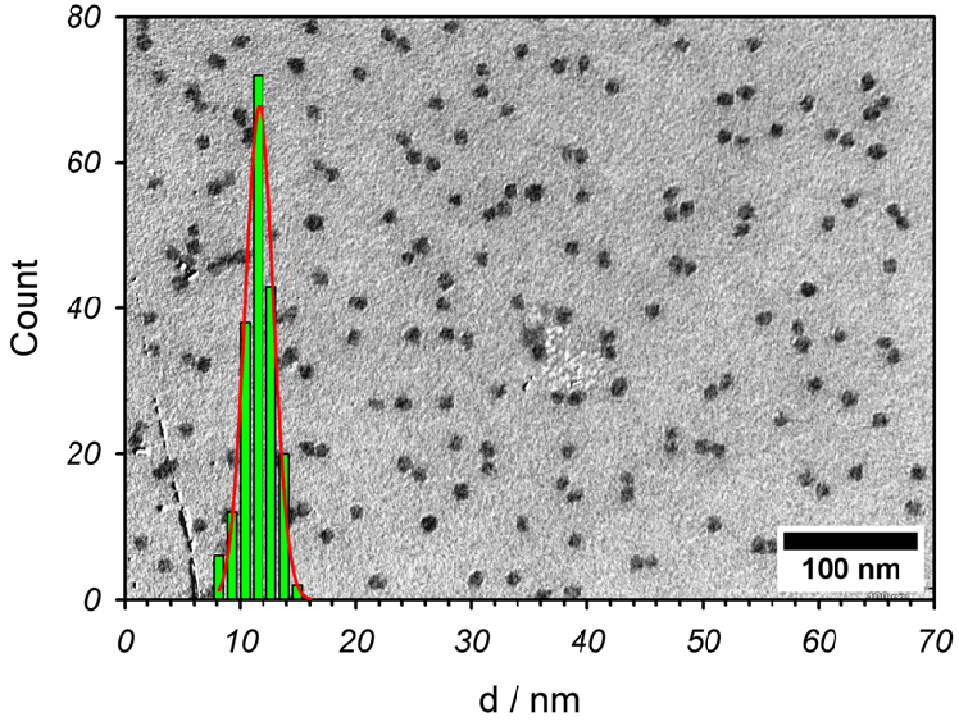

Figure S10: **NP-2**, TEM image and silica core size distribution: d = (12 ± 1) nm.

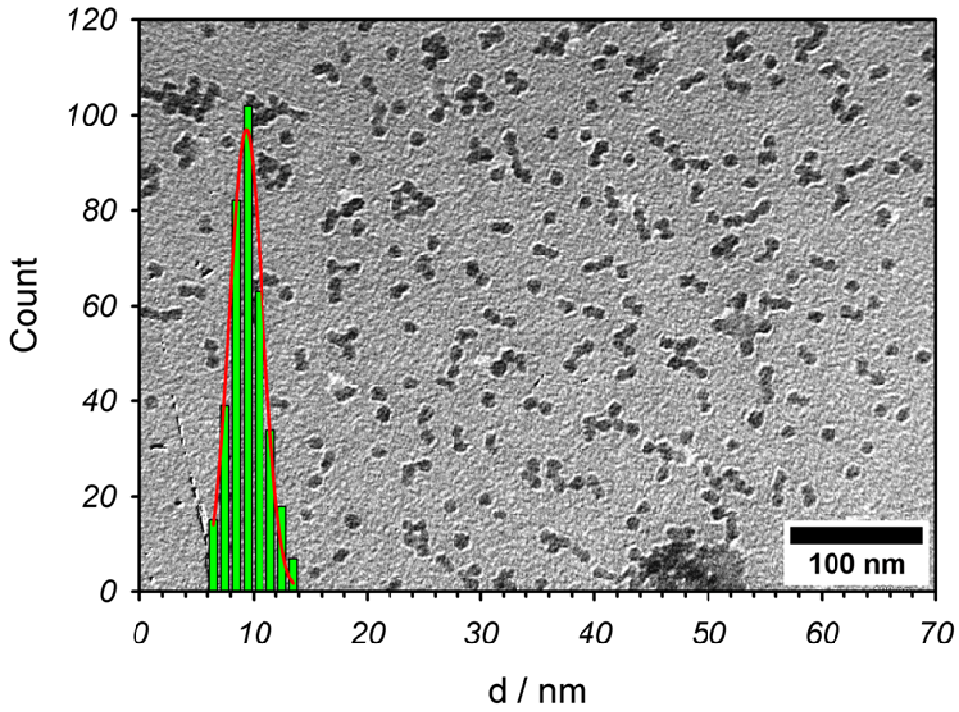

Figure S11: **NP-3**, TEM image and silica core size distribution: d = (9.3 ± 1.5) nm.

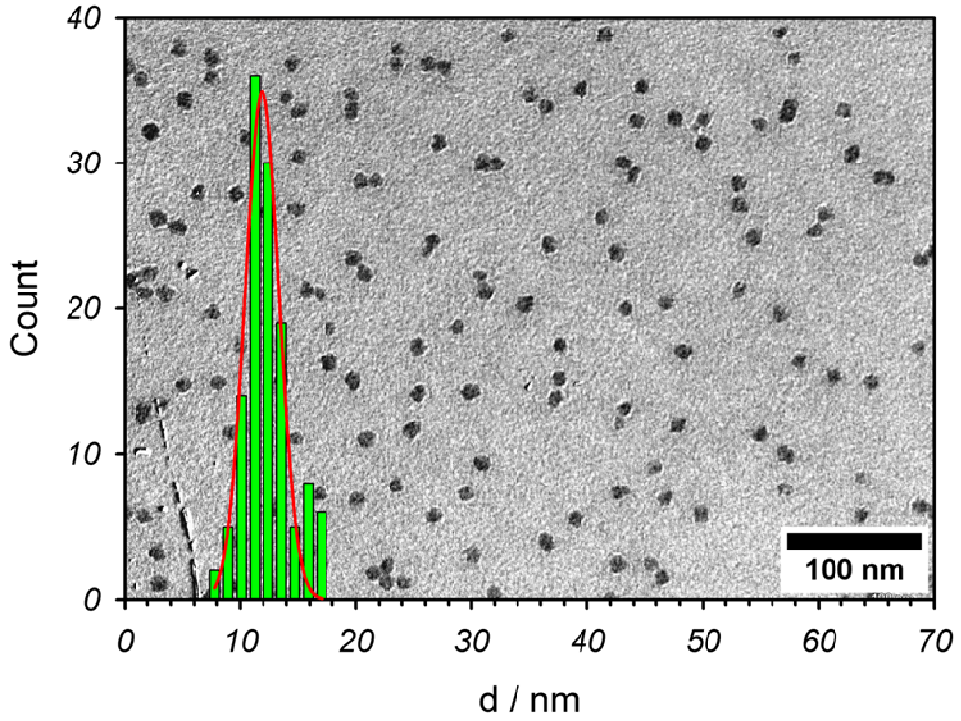

Figure S12: **NP-4**, TEM image and silica core size distribution: d = (12.0 ± 1.5) nm.

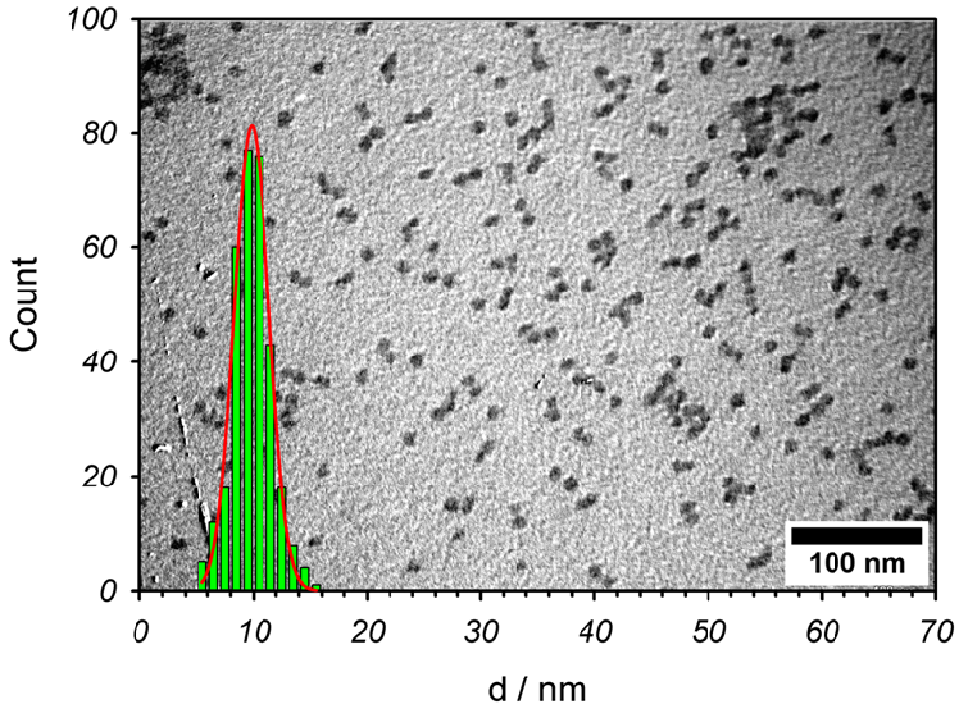

Figure S13: **NP-5**, TEM image and silica core size distribution: d = (9.8 ± 1.5) nm.

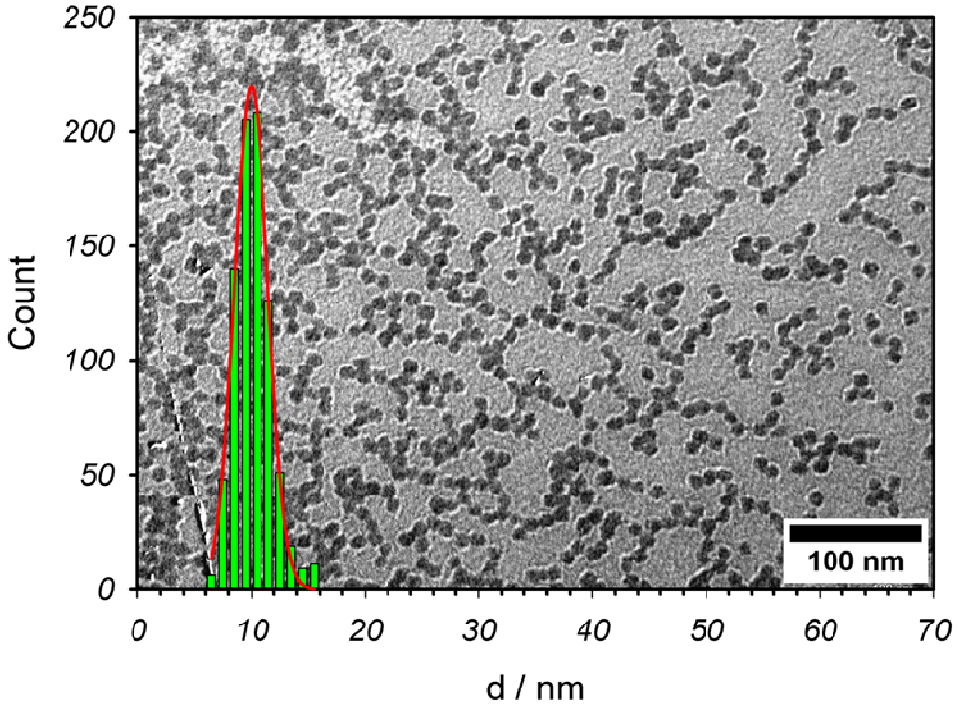

Figure S14: **NP-6**, TEM image and silica core size distribution: d = (10.0 ± 1.5) nm.

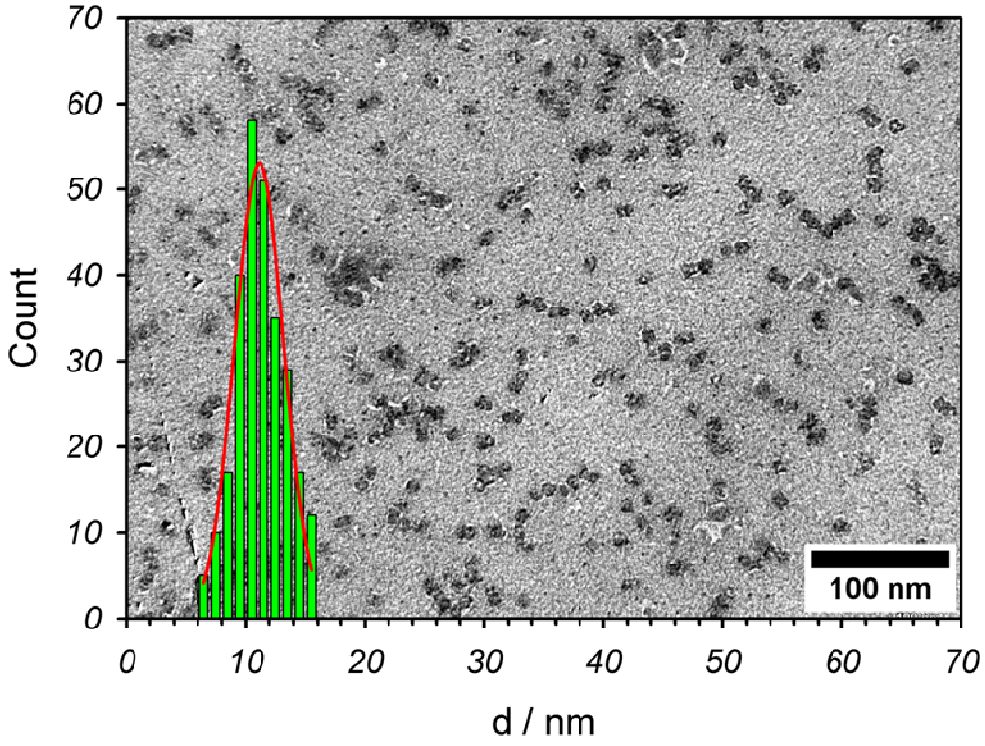

Figure S15: **NP-7**, TEM image and silica core size distribution: d = (11 ± 2) nm.

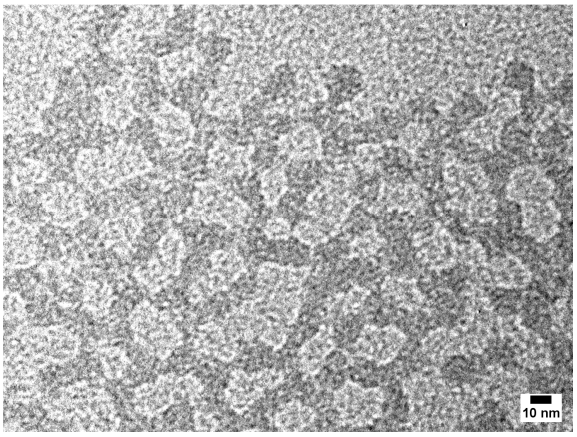

NP-1

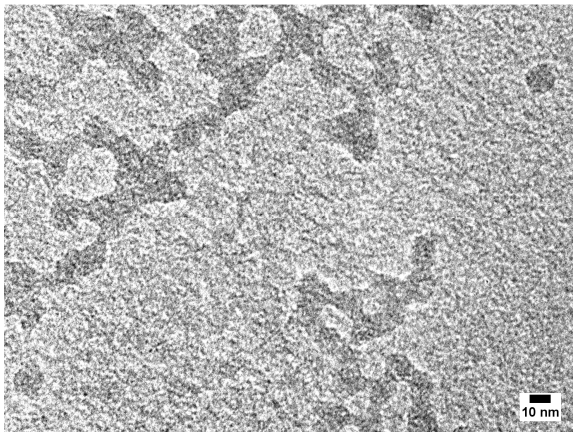

NP-2

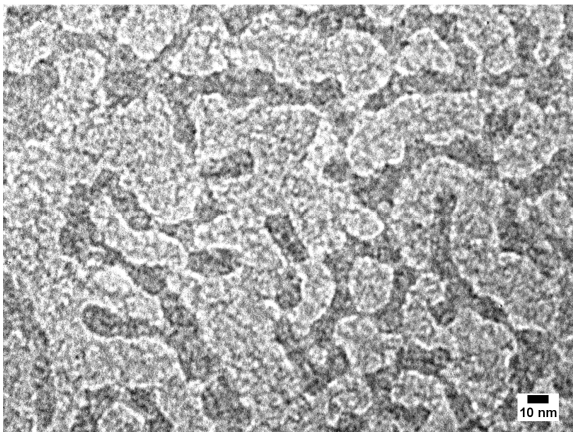

NP-3

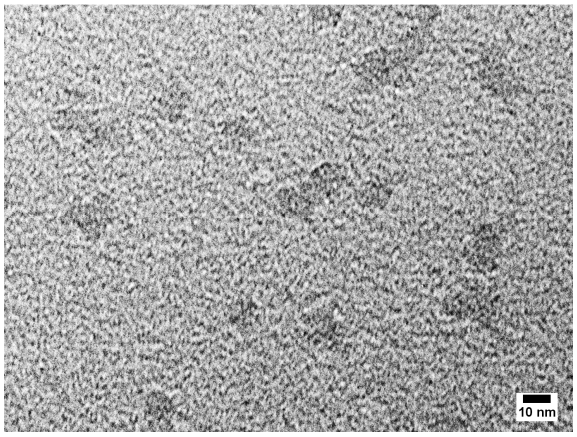

NP-4

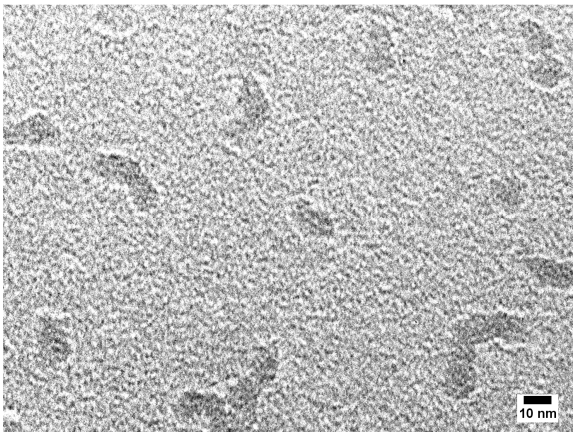

NP-5

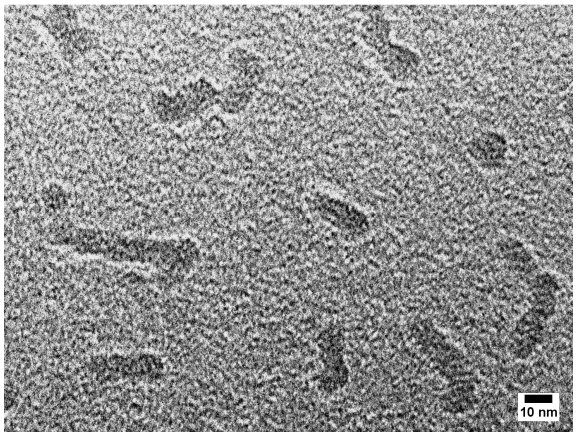

NP-6

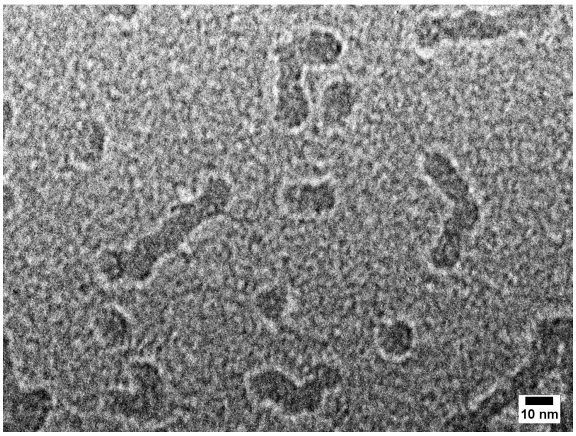

NP-7

Figure S16: Details of TEM images of nanoparticles samples, taken at 540000 magnification.

Dynamic Light Scattering (DLS)

NIR-Plus NPs hydrodynamic diameter (d_H) distributions were obtained in water at 25°C through DLS measurements using a Malvern Nano ZS instrument equipped with a 633 nm laser diode and a band pass filter centered at this wavelenght. Samples were filtered with 0.22 μm RC filters and then housed in disposable polystyrene cuvettes of 1 cm optical path length, using water as solvent. The width of DLS hydrodynamic diameter distribution is indicated by PdI (Polydispersion Index). In case of a mono-modal distribution (gaussian) calculated by means of cumulant analysis, $PdI=(\sigma/Z_{avg})^2$, where σ is the width of the distribution and Z_{avg} is average diameter of the particles population respectively. DLS measurements showed no aggregation of the NPs even after several months.

As shown by the TEM images, all the NIR-PluS NPs had very similar average silica core diameters. In some cases the average hydrodynamic diameter measured by DLS analysis was slightly higher than the expected average value (25-30 nm). The DLS technique over-weight the average size for a colloidal sample with moderate polydispersity (PdI = 0.2): for this reason the size distribution by volume are showed to represent a more realistic picture of the hydrodynamic diameter of the NIR-PluS NPs in solution.

Table S2: DLS Hydrodynamic diameter values in water for the nanoparticles samples described in this work. Standard deviation was calculated on five different measurements.

Sample	***d_H ± SD [nm]***	***PdI***
NP-1	41 ± 3	0.22
NP-2	42 ± 3	0.23
NP-3	41 ± 3	0.17
NP-4	28 ± 1	0.19
NP-5	33 ± 2	0.30
NP-6	29 ± 2	0.22
NP-7	28 ± 2	0.20

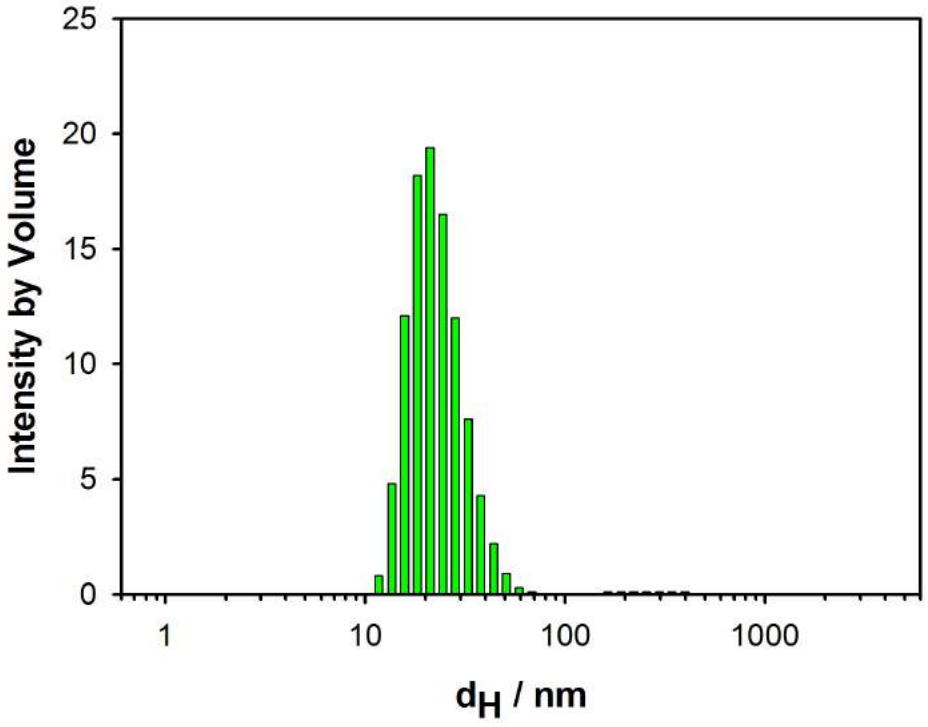

Figure S17: DLS diameter distribution by volume of **NP-1** (d_H = 41 ± 3 nm; water, 25°C).

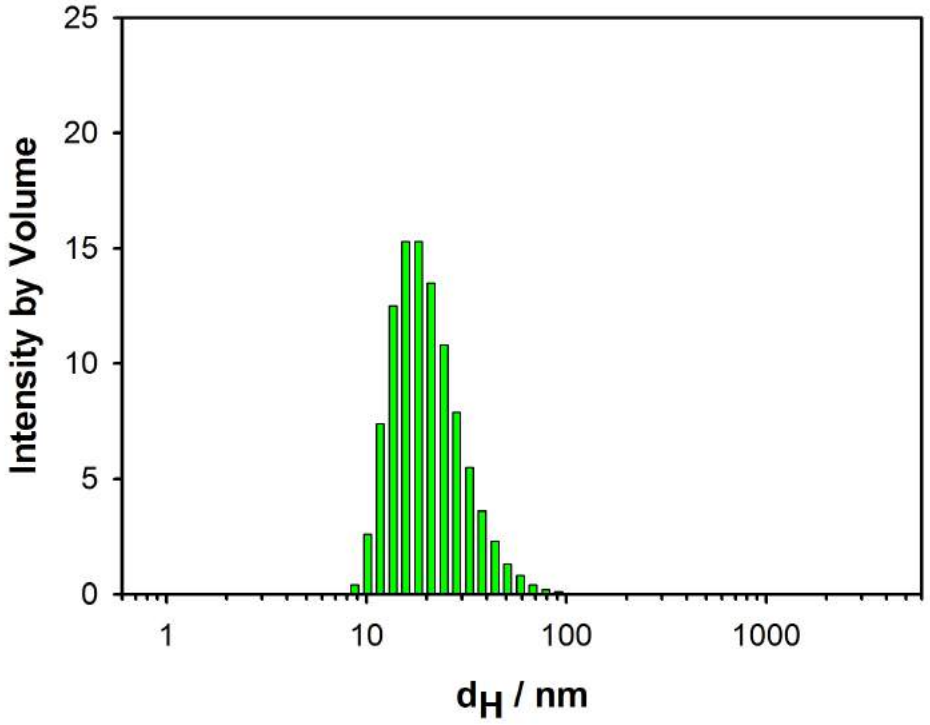

Figure S18: DLS diameter distribution by volume of **NP-2** (d_H = 42 ± 3 nm; water, 25°C).

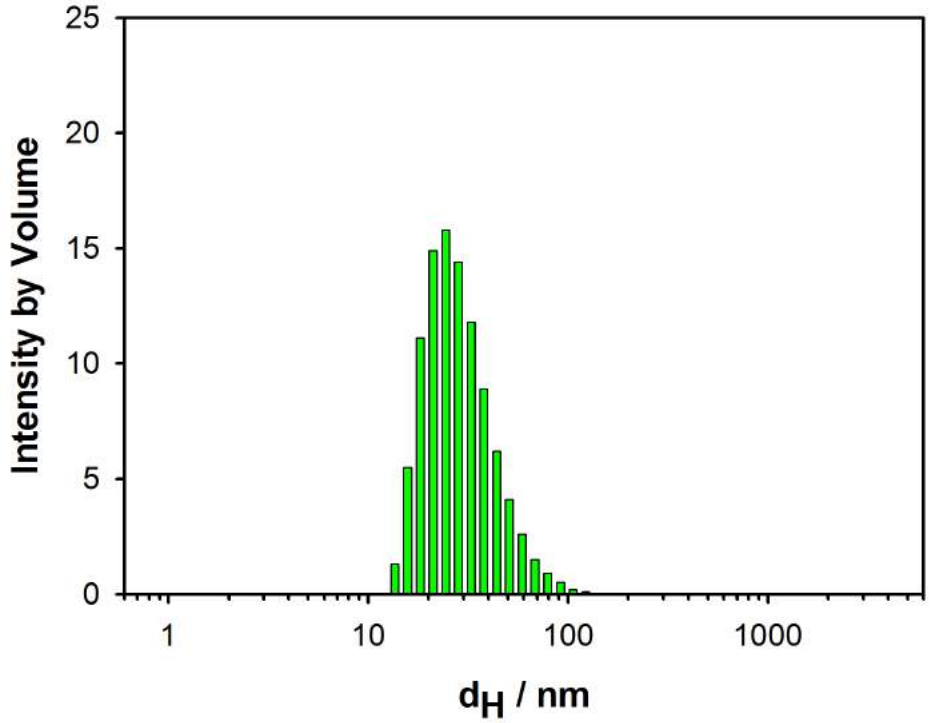

Figure S19: DLS diameter distribution by volume of **NP-3** (d_H = 41 ± 3 nm; water, 25°C).

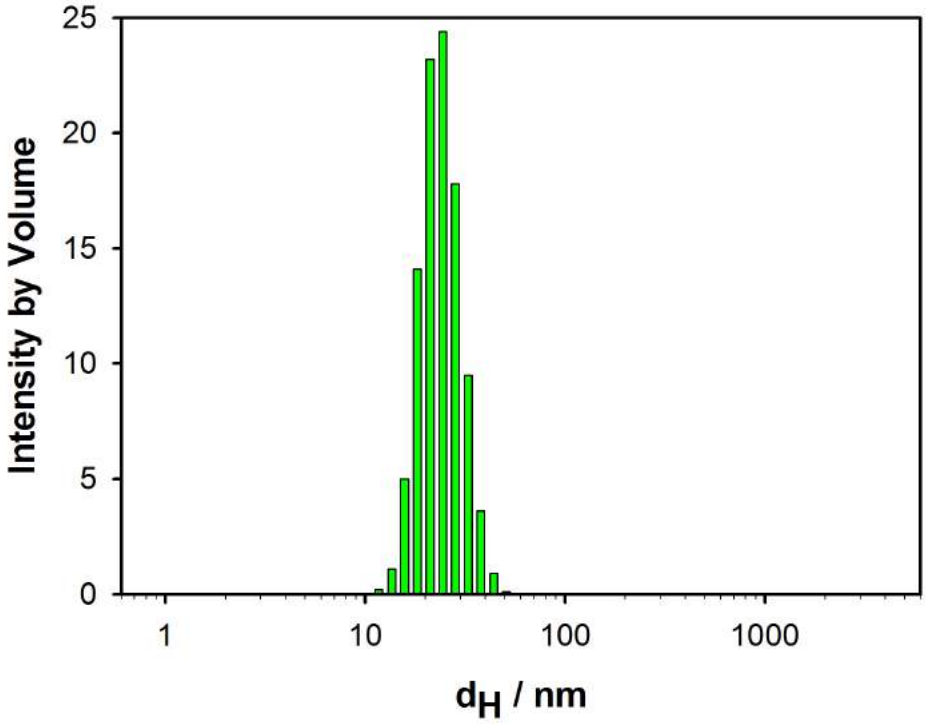

Figure S20: DLS diameter distribution by volume of **NP-4** (d_H = 28 ± 2 nm; water, 25°C).

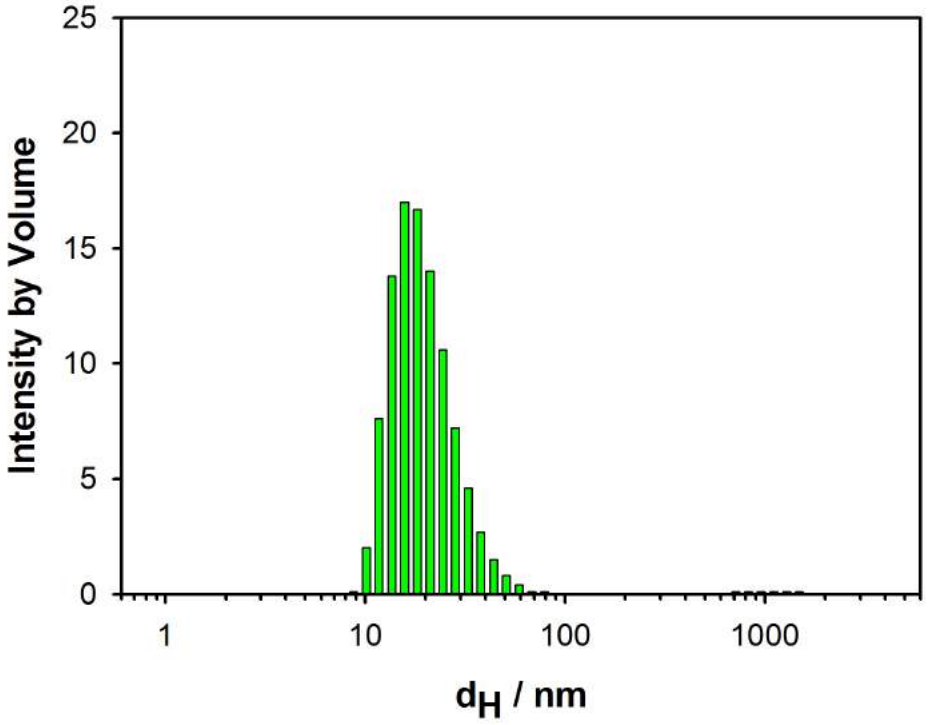

Figure S21: DLS diameter distribution by volume of **NP-5** (d_H = 33 ± 2 nm; water, 25°C).

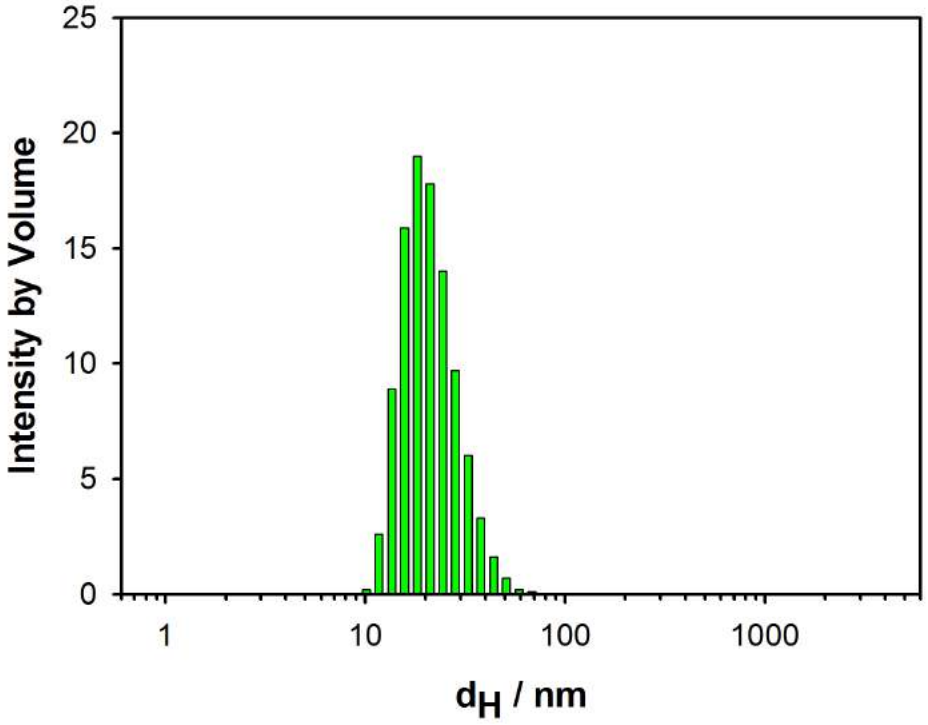

Figure S22: DLS diameter distribution by volume of **NP-6** (d_H = 29 ± 2 nm; water, 25°C).

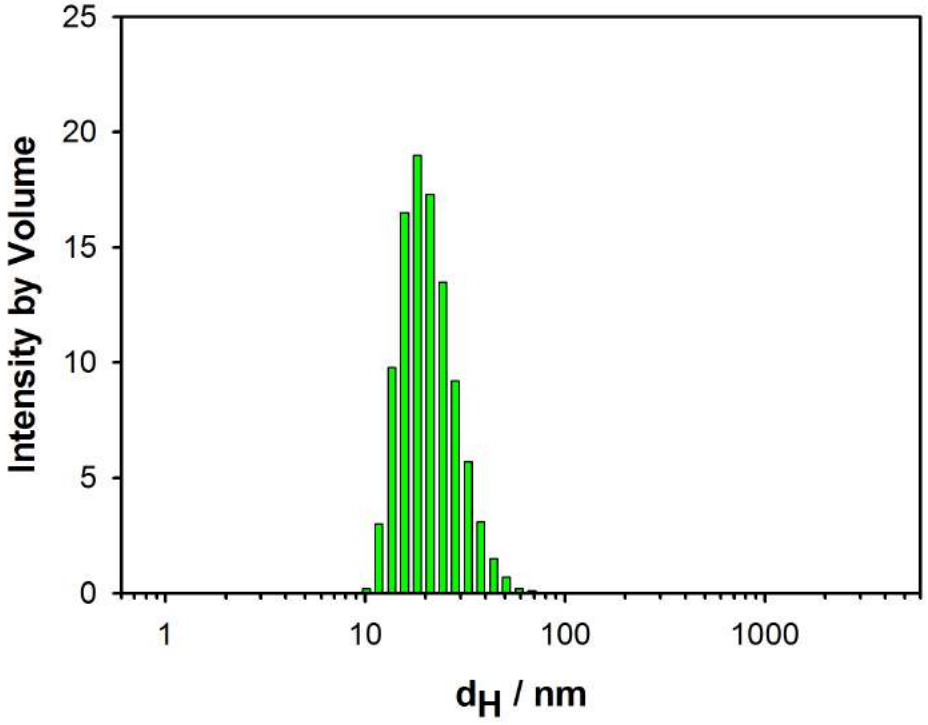

Figure S23: DLS diameter distribution by volume of **NP-7** (d_H = 28 ± 2 nm; water, 25°C).

References

1. Biffi S, Petrizza L, Rampazzo E, et al. Multiple dye-doped NIR-emitting silica nanoparticles for both flow cytometry and in vivo imaging. *RSC Adv.* 2014;4(35):18278-18285.
2. Helle M, Rampazzo E, Monchanin M, et al. Surface chemistry architecture of silica nanoparticles determine the efficiency of in vivo fluorescence lymph node mapping. *ACS Nano.* 2013;7(10):8645-8657.
3. Soper SA, Mattingly QL. Steady-State and Picosecond Laser Fluorescence Studies of Nonradiative Pathways in Tricarbocyanine Dyes: Implications to the Design of Near-IR Fluorochromes with High Fluorescence Efficiencies. *J. Am. Chem. Soc.* 1994;116(9):3744-3752.
4. Montalti M, Credi A, Prodi L, Gandolfi MT. *Handbook of Photochemistry.* 3rd Ed. ed. Boca Raton CRC Taylor & Francis; 2006.
5. Lakowicz JR. *Principles of Fluorescence Spectroscopy.* 3rd edition ed: Springer; 2006.